LAWRENCE
LIVERMORE
NATIONAL
LABORATORY

LLNL-JRNL-483427

A Fourth Order Accurate Finite Difference Scheme for the Elastic Wave Equation in Second Order Formulation

Bjorn Sjogreen and N. Anders Petersson

May 11, 2011

Submitted to Journal of Scientific Computing

Disclaimer

A fourth order accurate finite difference scheme for the elastic wave equation in second order formulation

Björn Sjögreen* and N. Anders Petersson*

May 11, 2011

Abstract

We present a fourth order accurate finite difference method for the elastic wave equation in second order formulation, where the fourth order accuracy holds in both space and time. The key ingredient of the method is a boundary modified fourth order accurate discretization of the second derivative with variable coefficient, $(\mu(x)u_x)_x$. This discretization satisfies a summation by parts identity that guarantees stability of the scheme. The boundary conditions are enforced through ghost points, thereby avoiding projections or penalty terms, which often are used with previous summation by parts operators. The temporal discretization is obtained by an explicit modified equation method. Numerical examples with free surface boundary conditions show that the scheme is stable for CFL-numbers up to 1.3, and demonstrate a significant improvement in efficiency over the second order accurate method. The new discretization of $(\mu(x)u_x)_x$ has general applicability, and will enable stable fourth order accurate approximations of other partial differential equations as well as the elastic wave equation.

1 Introduction

The benefits of higher order accurate schemes for wave propagation have been known for a long time [10, 8], but have mostly been developed for first order hyperbolic systems. For second order hyperbolic systems, higher order accurate finite difference schemes that satisfy the summation parts principle have only been developed for

*Center for Applied Scientific Computing, L-422, LLNL, P.O. Box 808, Livermore, CA 94551, USA. This work performed under the auspices of the U.S. Department of Energy by Lawrence Livermore National Laboratory under Contract DE-AC52-07NA27344.

constant coefficients [15]. In particular, it has not been known how to construct a provably stable, higher order accurate, finite difference scheme for the elastic wave equation that handles free surface boundary conditions and heterogeneous material properties.

We have previously developed second order accurate discretizations of the elastic wave equation, where the spatial discretization satisfies a summation by parts principle [16, 1, 20] that guarantees stability of the method. In the present paper, we generalize our techniques to fourth order of accuracy in both space and time. We construct a fourth order accurate finite difference approximations of second derivative terms such as $\partial/\partial x(\mu\partial u/\partial x)$, where $\mu > 0$ is a variable coefficient and u is the dependent variable. The discretization is consistent with previous summation by parts stencils for approximating first derivatives [12, 22, 3, 21], which can be combined to approximate cross-terms like $\partial/\partial y(\mu\partial u/\partial x)$. Our discretizations enforce the necessary relations between the stencils for the second derivatives and the cross terms. As a result, our scheme satisfies a discrete energy estimate, and is therefore energy stable. An additional benefit of our higher order discretization of $\partial/\partial x(\mu\partial u/\partial x)$ is that it is designed to use one ghost point outside of the computational domain. The solution value at this ghost point is determined by the discrete boundary condition. Hence, the boundary conditions can be enforced pointwise, instead of using the penalty terms of previous summation by parts schemes [2, 3]. We design the new discretization of second derivatives such that the requirements for obtaining an energy stable scheme are satisfied, independently of how the coefficient μ varies in space. This property also allows us to treat general curvilinear coordinate mappings.

Several numerical methods have previously been developed for solving the elastic wave equation. The fourth order staggered grid finite difference method proposed by Virieux [23], Levander [13], Graves [6], and others, has been used extensively for seismic wave simulations. This method discretizes the elastic wave equation as a first order hyperbolic system using the velocity-stress formulation. The method is fourth order accurate in space, but only second order in time. The method uses a regular Cartesian grid with constant grid spacing and is limited to flat topographies. Analysis of the stability of the method, e.g. [13], uses Fourier techniques and is limited to the periodic problem with homogeneous material properties.

The spectral element method was used by Komatitish and Tromp [9] to obtain a spatially high order approximation of the elastic wave equation in second order formulation. The stability of the spectral element method is obtained through the energy method, which also is used to prove stability of the finite difference method based on summation by parts operators. In the spectral element method, a different discretization stencil is used at each interior node point in each element, even on a regular Cartesian grid. In contrast, the summation by parts formulas only prescribe different stencils at a fixed number of points near a physical boundary. Because of

the clustering of internal node points near the element boundaries, spectral element methods must use a smaller explicit time step than finite difference methods of the same order of accuracy. To allow for realistic topographies and variable grid size, the spectral element method is often implemented on an unstructured hexahedral grid, which needs to be conforming. Compared to a finite difference method, the unstructured nature of the grid makes an efficient implementation more challenging, in particular on modern massively parallel machines. Furthermore, the generation of a high quality unstructured hexahedral grid can be difficult and time consuming.

Dumbser and Kaser [4] developed a high order accurate discontinuous Galerkin method for solving the elastic wave equation in first order formulation on an unstructured tetrahedral mesh. Compared to the conforming hexahedral mesh used in the spectral element method, a tetrahedral mesh allows for greater flexibility for treating complex geometries. A discontinuous Galerkin method on a non-conforming hexahedral mesh was used by Wilcox et al. [24] to solve the mixed elastic-acoustic wave equation in seismic applications. Allowing for hanging nodes significantly simplifies the mesh generation in seismic applications, where the grid size often only needs to depend on the depth below the topography. Similar to the spectral element method, the explicit time step restriction is considerably more limiting for the discontinuous Galerkin method compared to a finite difference method of comparable accuracy.

A spectral discretization of the first order formulation of the elastic wave equation was analyzed by Feng et al. [5]. The boundary conditions were enforced by a penalty term, and the material was assumed to be homogeneous.

The remainder of the paper is organized as follows. Basic properties of summation by parts operators are reviewed in section 2. In section 3, we derive a fourth order accurate summation by parts operator for approximating $\partial/\partial x(\mu\partial u/\partial x)$. In section 4, we use the new operator to discretize the elastic wave equation in space and time. We prove an energy estimate for the fully discrete problem. To simplify the presentation, we limit the analysis to two space dimensions with one periodic direction. From this description it is straightforward to generalize the results to three space dimensions with traction free or Dirichlet boundary conditions on different sides of the domain. Numerical experiments are presented in section 5, and conclusions are given in section 6.

2 Summation by parts operators for second derivatives

In [16], we presented a second order accurate finite difference discretization of the elastic wave equation in second order formulation. We were able to prove that the discrete energy is conserved by the scheme, for the equations with variable coefficients on a bounded domain with traction free or Dirichlet boundary conditions.

The spatial operator in the elastic wave equation consists of second derivative terms such as $(\mu u_x)_x$, and cross-terms like $(\mu u_y)_x$. The finite difference scheme in [16] uses a summation by parts finite difference operator, D_2, to approximate the first derivatives in the cross-terms, and another finite difference operator, G_2, to approximate the terms of the form $(\mu u_x)_x$. We exemplify these operators on a one-dimensional domain $0 \le x \le 1$, discretized by the grid points $j = 0, \ldots, N+1$, with boundaries at $j = 1$ and $j = N$. The constant grid spacing is $h = 1/(N-1)$. The operators used in [16] are given by

$$D_2 u_j = \begin{cases} (u_{j+1} - u_j)/h, & j = 1, \\ (u_{j+1} - u_{j-1})/(2h), & 2 \le j \le N-1, \\ (u_j - u_{j-1})/h, & j = N, \end{cases} \tag{1}$$

and

$$G_2(\mu) u_j = \frac{1}{h^2}\big(\mu_{j+1/2}(u_{j+1} - u_j) - \mu_{j-1/2}(u_j - u_{j-1})\big), \quad 1 \le j \le N.$$

Here, u_j is the approximation of $u(x_j)$, $\mu_j = \mu(x_j)$, and $\mu_{j+1/2} = (\mu_{j+1} + \mu_j)/2$. Note that values at the ghost points $j = 0$ and $j = N+1$ are not used by the operator D_2, but they do appear in the operator G_2. The operator (1) is second order accurate in the interior, first order on the boundary, and satisfies the summation by parts property

$$(u, D_2 v)_{hw2} = -(D_2 u, v)_{hw2} - u_1 v_1 + u_N v_N \tag{2}$$

in the weighted scalar product

$$(u, v)_{hw2} = \frac{h}{2} u_1 v_1 + h \sum_{j=2}^{N-1} u_j v_j + \frac{h}{2} u_N v_N. \tag{3}$$

The key identity for proving the discrete energy estimate in [16] is

$$\begin{aligned} \big(u, G_2(\mu) v\big)_{hw2} = -\big(D_2 u, \mu D_2 v\big)_{hw2} - \frac{h^2}{4}\big(D_+ D_- u, \mu D_+ D_- v\big)_{hr2} \\ - u_1(\mu_{1/2} D_+ v_0 + \mu_{3/2} D_+ v_1) \\ + u_N(\mu_{N+1/2} D_+ v_N + \mu_{N-1/2} D_+ v_{N-1}), \end{aligned} \tag{4}$$

where D_+ and D_- are the standard first order forward and backward divided difference operators. In the proof, the first term on the right hand side of (4) is combined with similar terms from the cross-terms to form the discrete energy. The last term on the first line (which uses a different scalar product) prevent highly oscillatory modes such as $(-1)^j$ from growing. The terms on the second and third line of (4)

are boundary terms. They cancel by appropriately chosen discretizations of the boundary conditions. For details on the derivation of the estimate, see [16, 17].

The objective of this article is to generalize the energy conserving second order accurate finite difference scheme in [16] to higher order accuracy. We do this by defining higher order versions of the operators D_2 and G_2, satisfying higher order versions of (2) and (4). Energy conservation then follows in exactly the same way as in the second order accurate case.

Higher order summation by parts operators for approximating first derivatives are well known, see for example [22]. Operators documented in the literature approximate the first derivative to pth order accuracy in the interior, and to order $p/2$ near the boundary, for $p = 2, 4, 6, 8, 10$. We will use these operators in place of D_2, with special focus on the case $p = 4$.

In this article we describe the derivation of a fourth order version of $G_2(\mu)$ that satisfies

$$\big(u, G(\mu)v)\big)_{hw} \;=\; -\big(Du, \mu Dv\big)_{hw} - \big(u, P(\mu)v\big)_h - u_1\mu_1 B_1 v_1 + u_N\mu_N B_N v_N. \quad (5)$$

This identity is of the same type as (4). Here D is the summation by parts operator approximating the first derivative to forth order accuracy. Note that the weights in the scalar product $(u, v)_{hw}$ depend on the order of accuracy and are related to the coefficients in D. The operator $P(\mu)$ is symmetric positive semi-definite, with a null space consisting of discretizations of low order polynomials of the spatial variable, i.e., functions that are very smooth on the grid. Similar to the second order accurate case, the term $(u, P(\mu)v)_h$ prevents poorly resolved modes from growing in time. $B_1 v_1$ and $B_N v_N$ are fourth order accurate approximations of $v_x(x_1)$ and $v_x(x_N)$, respectively.

By the notation a "pth order accurate operator", we mean a finite difference operator that is pth order accurate away from all boundaries, but where the accuracy may be reduced, usually to $p/2$, at a fixed number of points near the boundary. According to the theory in [7], the convergence rate of the numerical solution can be expected to be higher than $p/2$. For example, the discretization of the elastic wave equation that we develop below has a second order truncation error near the boundaries, but the numerical solution converges to the exact solution with fourth order convergence rate at all grid points.

3 Fourth order SBP operators for $(\mu u_x)_x$

The discussion in this section is restricted to one space dimension and directional superscripts on the difference operators are omitted. Generalization to more than one dimension is straightforward by using Cartesian products of the one-dimensional operators.

Assume that the grid is given by $x_j = (j-1)h$, $j = 0, 1, 2, \ldots$, where the boundary is located at x_1 and x_0 is a ghost point. Only the lower boundary is considered in this section. Conditions at the upper boundary follow in the same way. Let $u_j = u(x_j)$ denote a grid function. The weights in the discrete scalar product are denoted by the positive diagonal matrix Ω. For real valued grid functions u_j and v_j, the discrete scalar product on a semi-infinite domain is defined by

$$(u, v)_{hw+} = h \sum_{j=1}^{\infty} \omega_j u_j \, v_j, \quad \Omega = \mathrm{diag}(\omega_1, \omega_2, \ldots), \quad \omega_j > 0.$$

We will here focus on the summation by parts approximation that is fourth order accurate away from boundaries. The weights in the scalar product for this case has $\omega_j = 1$ for $j \geq 5$. Denote the fourth order approximation of $(\mu u_x)_x$ by $G(\mu)u$. For the case of a one-dimensional semi-infinite domain, identity (5) becomes

$$\big(u, G(\mu)v\big)_{hw+} = -\big(Du, \mu Dv\big)_{hw+} - \big(u, Pv\big)_{h+} - u_1 \mu_1 B v_1. \tag{6}$$

The operator P is positive semi-definite in the sense

$$\big(u, Pv\big)_{h+} = \big(Pu, v\big)_{h+}, \quad \big(u, Pu\big)_{h+} > 0, \quad u \notin \mathbb{P},$$

where $\mathbb{P}$ is a set of discretizations of low order polynomials. Since these are resolved modes, they will usually be excluded by properties of the particular partial differential equation that is being approximated. For real-valued grid functions u_j and v_j, the scalar product $(u, v)_{h+}$ is defined by

$$\big(u, v\big)_{h+} = h \sum_{j=1}^{\infty} u_j v_j, \quad \|u\|_{h+}^2 = \big(u, u\big)_{h+}.$$

The two scalar products are related by

$$\big(u, v\big)_{hw+} = \big(u, \Omega v\big)_{h+}.$$

Bu_1 is a fourth order accurate approximation of the boundary derivative $u_x(x_1)$, that uses the ghost point value u_0 with a non-zero weight. All computations in this article use the five point boundary operator

$$Bu_1 = \frac{1}{12h}(-3u_0 - 10u_1 + 18u_2 - 6u_3 + u_4) = u_x(x_1) + \mathcal{O}(h^4).$$

The summation by parts operator D approximates the first derivative to order four in the interior and to order two near the boundary. It will be needed in the approximation of the mixed terms $(\mu u_x)_y$. D, being the standard summation by parts

operator, does not use any ghost point values. For $j \geq 5$, Du_j is the five point wide, fourth order accurate, approximation of u_x,

$$Du_j = \frac{1}{12h}\left(-u_{j+2} + 8u_{j+1} - 8u_{j-1} + u_{j-2}\right) = u_x(x_j) + \mathcal{O}(h^4).$$

For $1 \leq j \leq 4$, Du_j is second order accurate, and its stencil uses the values $u_1, \ldots, u_6$. The exact form of D can be found in [22].

For the case of a one-dimensional semi-infinite domain, relation (2) becomes

$$\big(u, Dv\big)_{hw+} = -\big(Du, v\big)_{hw+} - u_1 v_1. \tag{7}$$

The summation by parts property (7) shows that

$$\big(u, G(\mu)v\big)_{hw+} = \big(u, D(\mu Dv)\big)_{hw+} - \big(u, Pv\big)_{h+} + u_1\mu_1 Dv_1 - u_1\mu_1 Bv_1, \tag{8}$$

is equivalent to (6).

In the interior of the domain, let $G(1)u_j$ denote the five point wide, fourth order accurate, approximation of u_{xx},

$$G(1)u_j = D_+D_-u_j - \frac{h^2}{12}\left(D_+D_-\right)^2 u_j.$$

Note that DDu_j is a nine point wide, fourth order accurate, approximation of u_{xx}. It is related to $G(1)u_j$ by

$$G(1)u_j = DDu_j + \frac{h^4}{18}(D_+D_-)^3 u_j - \frac{h^6}{144}(D_+D_-)^4 u_j.$$

Away from the boundary, we approximate $(\mu u_x)_x$ by

$$G(\mu)u_j = D(\mu_j Du_j) + \frac{h^4}{18}D_+D_-D_+(\mu_{j-1/2}D_-D_+D_-u_j) \\ - \frac{h^6}{144}(D_+D_-)^2(\mu_j(D_+D_-)^2 u_j). \tag{9}$$

Here, $\mu_{j-1/2} = (\mu_j + \mu_{j-1})/2$. It is straight forward to verify that formula (9) is a fourth order accurate, five point wide, operator in u_j.

One possible definition of a summation by parts operator for $(\mu u_x)_x$ is

$$\widetilde{G(\mu)}u_j = D(\mu_j Du_j) + \Omega^{-1}\Big(-\frac{h^6}{144}C_8(\mu)u_j + \frac{h^4}{18}C_6(\mu)u_j \\ + \delta_{1,j}(\mu_1 Du_1 - \mu_1 Bu_1)/h\Big), \tag{10}$$

where $\delta_{1,j} = 0$ for $j \neq 1$ and $\delta_{1,1} = 1$. Here, C_6 and C_8 are semi-bounded sixth and eight order difference operators, respectively. Away from the boundary,

$$C_6(\mu)u_j = D_+D_-D_+\left(\mu_{j-1/2}D_-D_+D_-u_j\right),$$
$$C_8(\mu)u_j = \left(D_+D_-\right)^2\left(\mu_j\left(D_+D_-\right)^2 u_j\right).$$

The operators C_6, C_8, and any C_{2q} of similar form can be boundary modified to satisfy

$$(-1)^{q+1}(u, C_{2q}u)_{h+} \leq 0, \tag{11}$$

in the l_2 discrete scalar product [21]. The boundary modification increases the magnitude of the operator C_{2q} to order $\mathcal{O}(1/h^q)$ near the boundary. In (10), the semi-bounded boundary modification of the sixth and eight differences are made with x_1 as the leftmost point. The ghost point is not used in these two terms.

By forming the scalar product between (10) and u_j, it is clear that property (8) holds. The semi-boundedness of the sixth and eight difference terms lead to a positive semi-definite P in (8).

The local truncation error in (10) is only first order accurate near the boundary. Numerical experiments where this operator is used to solve the wave equation indicate a third order convergence rate for the solution. This is to be expected, because the first order truncation errors only occur near the boundary, and two orders of accuracy are gained when solving a hyperbolic equation in second order differential form. The gain in order only holds for numerical boundary conditions. The fourth order operator B should be used to approximate derivatives in the physical boundary conditions.

If the local truncation error at the boundary can be improved from first order to second order accuracy, we would obtain a method with fourth order convergence rate. There are three sources of first order truncation errors in (10). The term $D(\mu_j Du_j)$ is first order accurate near the boundary because Du is only a second order accurate approximation of u_x near the boundary. One order of accuracy is lost by applying the operator twice, since the truncation error of D is non-smooth. Secondly, the sixth difference $C_6(\mu)u_j$ is only a third order difference near the boundary, because of the semi-bounded boundary closure. This term results in a first order truncation error. Thirdly, the boundary term $\mu_1 Du_1/h$ has a first order error, because D is second order accurate on the boundary and one order is lost by dividing it by h.

It is possible to achieve second order accuracy at the boundary by splitting the sixth difference operator into four terms. We define

$$\begin{aligned} G(\mu)u_j = D(\mu_j Du_j) + \Omega^{-1}\Big(&-\frac{h^6}{144}C_8(\mu)u_j \\ &+ \alpha_1 h^4 C_{6,1}(\mu)u_j + \alpha_2 h^4 C_{6,2}(\mu)u_j + \alpha_3 h^4 C_{6,3}(\mu)u_j + \alpha_4 h^4 C_{6,4}(\mu)u_j \\ &+ \delta_{1,j}(\mu_1 Du_1 - \mu_1 Bu_1)/h\Big), \quad j \geq 1. \end{aligned} \tag{12}$$

where $C_{6,k}(\mu)u_j$ denotes the semi-bounded sixth difference operator that has x_k as its leftmost point. More specifically,

$$h^4 C_{6,k}(\mu)u_j = \begin{cases} 0, & j < k, \\ h\big(\mu_{k+3/2}D_-D_+D_-u_{k+2}\big), & j = k, \\ h\big(\mu_{k+5/2}D_-D_+D_-u_{k+3} - 3\mu_{k+3/2}D_-D_+D_-u_{k+2}\big), & j = k+1, \\ h\big(\mu_{k+7/2}D_-D_+D_-u_{k+4} - 3\mu_{k+5/2}D_-D_+D_-u_{k+3} & \\ \quad +3\mu_{k+3/2}D_-D_+D_-u_{k+2}\big), & j = k+2, \\ h^4 D_+D_-D_+\big(\mu_{j-1/2}D_-D_+D_-u_j\big), & j \geq k+3. \end{cases} \tag{13}$$

Using this notation, the sixth difference operator in (10) equals $C_{6,1}(\mu)u_j$. The boundary terms are consistent with a coefficient times $h\mu u_{xxx}$. This is of the same form as the truncation errors of $D(\mu Du)$, since Taylor expansion gives

$$D(\mu_j Du_j) = (\mu u_x)_x(x_j) + \begin{cases} c_j h\mu_j u_{xxx}(x_j) + \mathcal{O}(h^2) & j = 1, 2, \ldots, 6, \\ \mathcal{O}(h^4) & j \geq 7. \end{cases} \tag{14}$$

Similarly, let d_j denote the coefficients in the truncation error of order h^2 in the first difference operator, i.e.,

$$Du_j = u_x(x_j) + \begin{cases} d_j h^2 u_{xxx}(x_j) + \mathcal{O}(h^3) & j = 1, 2, \ldots, 4, \\ \mathcal{O}(h^4) & j \geq 5. \end{cases} \tag{15}$$

The coefficients c_j and d_j are given in Appendix A. We will let c and d denote grid functions c_j and d_j respectively, where $c_j = 0$ for $j \geq 7$ and $d_j = 0$ for $j \geq 5$.

The operator (12) is boundary modified for $j \leq 6$ and coincides with the five point wide operator (9) for $j \geq 7$. The α_j are coefficients that we now will determine such that all first order truncation errors cancel at the boundary points. Taylor expansion for the local truncation errors gives six equations that have to be satisfied, one equation for each of the grid points x_j, $j = 1, \ldots, 6$. The $\mathcal{O}(h)$ terms in first two equations are

$$c_1\mu_1 u_{xxx}(x_1) + \frac{1}{\omega_1}\left(\alpha_1\mu_{5/2}u_{xxx}(x_{5/2}) + \mu_1 d_1 u_{xxx}(x_1)\right) = 0,$$

$$c_2\mu_2 u_{xxx}(x_2) + \frac{1}{\omega_2}\left(\alpha_1\mu_{7/2}u_{xxx}(x_{7/2}) - 3\alpha_1\mu_{5/2}u_{xxx}(x_{5/2}) + \alpha_2\mu_{7/2}u_{xxx}(x_{7/2})\right) = 0.$$

Since u_{xxx} and μ are smooth functions of x, we can shift these coefficients and only commit a second order error. For example,

$$hu_{xxx}(x_{5/2}) = hu_{xxx}(x_1) + \mathcal{O}(h^2), \quad h\mu(x_{5/2}) = h\mu(x_1) + \mathcal{O}(h^2).$$

We can therefore recenter the variable coefficients and the third derivatives, in such a way that they can be removed from the equations. The final system for second order accuracy becomes

$$\begin{aligned}
\omega_1 c_1 + \alpha_1 + d_1 &= 0 \\
\omega_2 c_2 - 2\alpha_1 + \alpha_2 &= 0 \\
\omega_3 c_3 + \alpha_1 - 2\alpha_2 + \alpha_3 &= 0 \\
\omega_4 c_4 + \alpha_2 - 2\alpha_3 + \alpha_4 &= 0 \\
c_5 + \alpha_3 - 2\alpha_4 &= 0 \\
c_6 + \alpha_4 &= 0
\end{aligned} \tag{16}$$

This system has six equations and four unknowns. Nevertheless, the following theorem shows that (16) has a solution.

Theorem 1. *The system (16) has the unique solution*

$$\begin{aligned}
\alpha_1 &= 181507/1719312, \quad \alpha_2 = -1441/39984, \\
\alpha_3 &= -2593/151704, \quad \alpha_4 = 11/3528.
\end{aligned}$$

Furthermore, the positivity conditions

$$\alpha_1 > 0, \quad \alpha_1 + \alpha_2 > 0, \quad \alpha_1 + \alpha_2 + \alpha_3 > 0, \tag{17}$$

hold and

$$\alpha_1 + \alpha_2 + \alpha_3 + \alpha_4 = 1/18,$$

which agrees with the coefficient of the sixth difference in the interior from (9).

Proof. The theorem can easily be verified by inserting the solution into (16) and by explicitly evaluating the sums. However, since it might seem as pure luck that the overdetermined system (16) has a solution, we make an explicit derivation of the solution in Appendix B. The purpose of this derivation is to gain insight into how the properties of the summation by parts operator and scalar product make the conditions for solvability satisfied. □

The following theorem summarizes the properties of the difference operator $G(\mu)u_j$ defined by (12).

Theorem 2. *Assume that $\mu > 0$. The operator (12) with the values of α_j given in Theorem 1 is an approximation of $(\mu u_x)_x$ that is second order accurate near the boundary and fourth order accurate away from the boundary. Furthermore, it satisfies (8) with a positive semi-definite P. Furthermore, $(u, Pu)_{h+} = 0$ only for functions that are discretizations of quadratic polynomials.*

Proof. Theorem 1 shows that the order of accuracy is two near the boundary. The operator away from the boundary is identical to the fourth order stencil (9), because the sum of α_j is 1/18. Taking the scalar product between (12) and u_j shows that (8) holds with

$$(u, Pu)_{h+} = -h^4 \sum_{k=1}^{4} \alpha_k (u, C_{6,k}(\mu)u)_{h+} + \frac{h^6}{144}(u, C_8(\mu)u)_{h+}.$$

We know that $(u, C_{6,k}(\mu)u)_{h+} \leq 0$ and $(u, C_8(\mu)u)_{h+} \geq 0$ by the semi-bounded property (11) and because $\mu > 0$. A closer examination of the sixth difference terms shows that

$$(u, C_{6,k}(\mu)u)_{h+} = -\sum_{j=k+2}^{\infty} \mu_{j-1/2}(D_-D_+D_-u_j)^2$$

and hence,

$$\begin{aligned} -\sum_{k=1}^{4} \alpha_k (u, C_{6,k}(\mu)u)_{h+} &= \alpha_1 \mu_{3-1/2}(D_-D_+D_-u_3)^2 \\ &+ (\alpha_1+\alpha_2)\mu_{4-1/2}(D_-D_+D_-u_4)^2 + (\alpha_1+\alpha_2+\alpha_3)\mu_{5-1/2}(D_-D_+D_-u_5)^2 \\ &+ (\alpha_1+\alpha_2+\alpha_3+\alpha_4)\sum_{j=6}^{\infty} \mu_{j-1/2}(D_-D_+D_-u_j)^2. \quad (18) \end{aligned}$$

By the positivity conditions stated in Theorem 1, (18) is non-negative. Consequently, $(u, Pu)_{h+} \geq 0$. It is evident that if $(u, Pu)_{h+} = 0$ then

$$h^3 D_-D_+D_-u_j = u_{j+1} - 3u_j + 3u_{j-1} - u_{j-2} = 0. \quad j \geq 3$$

This difference equation has the solution $u_j = \gamma_0 + \gamma_1 j + \gamma_2 j^2$, $j \geq 1$, for constants $\gamma_0, \gamma_1, \gamma_2$, since 1 is a triple root of its characteristic polynomial. □

The property that $(u, Pu)_{h+} = 0$ only holds for well resolved modes is important for obtaining stability for difference schemes. For example, if the difference operator (12) would be used to approximate the second derivative in a diffusion problem, it means that there are no spurious numerical modes that are not diffused by the scheme.

Symbolic formula manipulation software can be used to explicitly evaluate the coefficient tensor $\beta_{j,k,m}$ of size $6 \times 8 \times 8$, such that

$$G(\mu)u_j = \sum_{k=1}^{8}\sum_{m=1}^{8} \beta_{j,k,m}\mu_m u_k, \quad j = 1, \ldots, 6. \quad (19)$$

In this expression, 129 out of the 384 entries in $\beta_{j,k,m}$ are non-zero.

Note that $G(\mu)u_j$ is different from the interior stencil (9) at grid points $j = 1, 2, \ldots, 6$. This is true also in the case when μ is constant. Therefore, (19) is different from the fourth order accurate summation by parts operator for u_{xx} given in [14], which only has a four point boundary modification.

The construction of the boundary modified sixth and eight order accurate summation by parts operators for $(\mu u_x)_x$ can be carried out in exactly the same way as presented for the fourth order case above, but is algebraically very involved. Also in these cases, the optimal boundary accuracy is achieved by solving overdetermined linear systems of equations for coefficients α multiplying higher difference operators that start at different points near the boundary, similar to the sum of sixth order differences

$$\alpha_1 C_{6,1}(\mu)u_j + \alpha_2 C_{6,2}(\mu)u_j + \alpha_3 C_{6,3}(\mu)u_j + \alpha_4 C_{6,4}(\mu)u_j,$$

used above. An additional difficulty for the sixth and eight order operators is that there are free parameters in the difference operator D. The sixth order operator has one free parameter and the eight order operator has three free parameters. It turns out that the positivity conditions corresponding to (17) are satisfied only for certain ranges of the free parameters. Care has to be taken when selecting them.

4 Energy conserving 4th order approximation of the elastic wave equation

This section describes and analyzes a fourth order discretization of the elastic wave equations, based on the summation-by-parts operators described in the previous section. For clarity of presentation, the description and analysis is done in two space dimensions with y-periodicity. It is straightforward to generalize the results to the three dimensional equations with either Dirichlet or traction free boundary conditions on any of the six sides, in the same way as in our previous work on the second order accurate discretization, see [16, 17]. The mathematical structure of the present fourth order discretization is exactly the same as in the second order discretization in [16].

We consider the elastic wave equation in two space dimensions,

$$\rho u_{tt} = ((2\mu + \lambda)u_x + \lambda v_y)_x + (\mu v_x + \mu u_y)_y + f^{(x)}, \tag{20}$$

$$\rho v_{tt} = (\mu v_x + \mu u_y)_x + (\lambda u_x + (2\mu + \lambda)v_y)_y + f^{(y)}, \tag{21}$$

on the Cartesian domain $0 \le x \le a$, $0 \le y \le b$. The displacements $u = u(x, y, t)$ and $v = v(x, y, t)$ in the x- and y-directions will sometimes be written in vector notation, $\mathbf{u} = (u\ v)$. The density $\rho = \rho(x, y)$ and the Lamé parameters $\lambda = \lambda(x, y)$

and $\mu = \mu(x, y)$ are assumed to be known. $\mathbf{F} = (f^{(x)}\ f^{(y)})$ is the external forcing. Initial data are given for the displacements and the velocities,

$$\mathbf{u}(x, y, 0) = \mathbf{g}_1, \qquad \mathbf{u}_t(x, y, 0) = \mathbf{g}_2,$$

with prescribed functions $\mathbf{g}_1$ and $\mathbf{g}_2$. The boundary conditions are periodic in the y-direction with homogeneous Dirichlet conditions at $x = 0$,

$$\mathbf{u}(0, y, t) = \mathbf{0}. \tag{22}$$

The boundary condition at $x = a$ is the normal stress condition

$$(2\mu + \lambda)u_x + \lambda v_y = \tau^{(xx)}, \tag{23}$$

$$\mu(v_x + u_y) = \tau^{(xy)}, \tag{24}$$

where $\tau^{(xx)}$ and $\tau^{(xy)}$ are functions of y and t. When $\tau^{(xx)} = \tau^{(xy)} = 0$ this boundary condition is often called a free surface, or traction free, condition.

We discretize (20),(21) on the grid $x_i = (i-1)h$, $y_j = (j-1)h$, for $0 \le i \le N_x+1$, $-1 \le j \le N_y + 1$. The domain sizes and the uniform grid spacing $h > 0$ are defined such that $x_{N_x} = a$ and $y_{N_y} = b$. The points outside the domain ($i = 0$, $i = N_x + 1$, $j = -1, 0$, $j = N_y+1$) are ghost points, which are used to simplify the discretization of the boundary conditions. Denote the displacements at grid point (x_i, y_j) at time t by $u_{i,j}(t)$ and $v_{i,j}(t)$ respectively. The discretization of the spatial derivatives in (20), (21), denoted by $L_h^{(u)}$ and $L_h^{(v)}$, is defined by

$$\begin{aligned} L_h^{(u)}(u_{i,j}, v_{i,j}) &= G^{(x)}(2\mu + \lambda)u_{i,j} + D^{(x)}(\lambda D^{(y)} v_{i,j}) + D^{(y)}(\mu D^{(x)} v_{i,j}) \\ &\quad + G^{(y)}(\mu)u_{i,j}, \end{aligned} \tag{25}$$

$$\begin{aligned} L_h^{(v)}(u_{i,j}, v_{i,j}) &= G^{(x)}(\mu)v_{i,j} + D^{(x)}(\lambda D^{(y)} u_{i,j}) + D^{(y)}(\mu D^{(x)} u_{i,j}) \\ &\quad + G^{(y)}(2\mu + \lambda)v_{i,j}. \end{aligned} \tag{26}$$

The semi-discrete finite-difference approximation becomes

$$\rho_{i,j} \frac{d^2 u_{i,j}}{dt^2} = L_h^{(u)}(u_{i,j}, v_{i,j}) + f_{i,j}^{(x)} \tag{27}$$

$$\rho_{i,j} \frac{d^2 v_{i,j}}{dt^2} = L_h^{(v)}(u_{i,j}, v_{i,j}) + f_{i,j}^{(y)}, \tag{28}$$

for $1 \le i \le N_x$, $1 \le j \le N_y - 1$. The finite difference operators $G^{(x)}(\mu)u$ and $D^{(x)}u$ approximate $(\mu u_x)_x$ and u_x respectively, with summation-by-parts boundary modifications, as described in the previous section. The y-direction operators

are similar, but without boundary modifications because of the y-periodicity. The periodic boundary conditions for the discretized variables are

$$u_{i,-1} = u_{i,N_y-2}, \qquad u_{i,0} = u_{i,N_y-1}, \qquad u_{i,N_y} = u_{i,1}, \qquad u_{i,N_y+1} = u_{i,2}, \tag{29}$$

$$v_{i,-1} = v_{i,N_y-2}, \qquad v_{i,0} = v_{i,N_y-1}, \qquad v_{i,N_y} = v_{i,1}, \qquad v_{i,N_y+1} = v_{i,2}, \tag{30}$$

for $0 \leq i \leq N_x + 1$. The Dirichlet condition (22) is imposed by

$$u_{1,j} = v_{1,j} = 0, \quad 1 \leq j \leq N_y - 1. \tag{31}$$

At first glance, this appears to not be a condition on the ghost point values $u_{0,j}$ and $v_{0,j}$. However, (31) can be imposed by determining $u_{0,j}$ and $v_{0,j}$ in such a way that (20) and (21), when applied at $(1, j)$, give (31). The structure of the operator (12) shows that the ghost point values only enter $G^{(x)}$ through the boundary operator $B^{(x)}$. Therefore the ghost point values are only used by $G^{(x)}$ at the boundary point $i = 1$. Because $u_{0,j}$ and $v_{0,j}$ are not used in any other computation, imposing (31) directly is equivalent to the more complicated procedure of first determining the ghost point values and then applying the difference scheme to obtain (31). The discretization of the normal stress boundary condition is provided by the fourth order accurate formulas

$$(2\mu + \lambda)_{N_x,j} B^{(x)} u_{N_x,j} + \lambda_{N_x,j} D^{(y)} v_{N_x,j} = \tau_j^{(xx)}(t), \tag{32}$$

$$\mu_{N_x,j} (B^{(x)} v_{N_x,j} + D^{(y)} u_{N_x,j}) = \tau_j^{(xy)}(t), \tag{33}$$

for $1 \leq j \leq N_y - 1$. Because $B^{(x)}$ uses the ghost point, it is straightforward to solve (32) and (33) for $u_{N_x+1,j}$ and $v_{N_x+1,j}$ respectively.

Denote the spatial discretization on vector form by $\mathbf{L}_h(\mathbf{u}) = (L_h^{(u)}(u, v)\, L_h^{(v)}(u, v))$. Energy estimation in our previous work for second order accurate methods, e.g., [17], has relied on the property

$$(\mathbf{u}^0, \mathbf{L}_h(\mathbf{u}^1))_{hw} = -S_h(\mathbf{u}^0, \mathbf{u}^1) + T_h(\mathbf{u}^0, \mathbf{u}^1), \tag{34}$$

for the spatial discretization. The bilinear form $S_h(\mathbf{u}^0, \mathbf{u}^1)$ is symmetric and positive semi-definite. $T_h(\mathbf{u}^0, \mathbf{u}^1)$ is also bilinear and consists of boundary terms. The scalar products used here,

$$(u, v)_{hw} = h^2 \sum_{j=1}^{N_y-1} \sum_{i=1}^{N_x} \omega_i u_{i,j} v_{i,j}, \quad (u, v)_h = h^2 \sum_{j=1}^{N_y-1} \sum_{i=1}^{N_x} u_{i,j} v_{i,j},$$

are the same as in Section 3, but on a bounded domain in two space dimensions. Since the y-direction is periodic, $(u, v)_{hw}$ is weighted only in the x-direction. We next prove that (34) holds also in the fourth order case.

Theorem 3. *The fourth order spatial discretization (25), (26) with periodic y-direction satisfies identity (34) with*

$$\begin{aligned} S_h(\mathbf{u}^0,\mathbf{u}^1) &= (\lambda(D^{(x)}u^0+D^{(y)}v^0), D^{(x)}u^1+D^{(y)}v^1)_{hw} + (2\mu D^{(x)}u^0, D^{(x)}u^1)_{hw} \\ &+ (\mu(D^{(x)}v^0+D^{(y)}u^0), D^{(x)}v^1+D^{(y)}u^1)_{hw} + (2\mu D^{(y)}u^0, D^{(y)}u^1)_{hw} \\ &+ (u^0, P^{(x)}(2\mu+\lambda)u^1)_h + (u^0, P^{(y)}(\mu)u^1)_h \\ &+ (v^0, P^{(y)}(2\mu+\lambda)v^1)_h + (v^0, P^{(x)}(\mu)v^1)_h, \end{aligned} \tag{35}$$

and

$$\begin{aligned} T_h(\mathbf{u}^0,\mathbf{u}^1) &= -\sum_{j=1}^{N_y-1} u^0_{1,j}((2\mu+\lambda)_{1,j}B^{(x)}u^1_{1,j} + \lambda_{1,j}D^{(y)}v^1_{1,j}) \\ &+ \sum_{j=1}^{N_y-1} u^0_{N_x,j}((2\mu+\lambda)_{N_x,j}B^{(x)}u^1_{N_x,j} + \lambda_{N_x,j}D^{(y)}v^1_{N_x,j}) \\ &- \sum_{j=1}^{N_y-1} v^0_{1,j}(\mu_{1,j}B^{(x)}v^1_{1,j} + \mu_{1,j}D^{(y)}u^1_{1,j}) \\ &+ \sum_{j=1}^{N_y-1} v^0_{N_x,j}(\mu_{N_x,j}B^{(x)}v^1_{N_x,j} + \mu_{N_x,j}D^{(y)}u^1_{N_x,j}). \end{aligned} \tag{36}$$

Furthermore, the boundary conditions (31), (32), and (33) with zero forcing imply that $T_h = 0$.

Proof. The left hand side of (34) can be written

$$(\mathbf{u}^0, \mathbf{L}_h(\mathbf{u}^1))_{hw} = (u^0, L_h^{(u)}(u^1,v^1))_{hw} + (v^0, L_h^{(v)}(u^1,v^1))_{hw}. \tag{37}$$

Fully written out, the first term in the right hand side of (37) is a sum of four terms,

$$\begin{aligned} (u^0, L_h^{(u)}(u^1,v^1))_{hw} &= (u^0, G^{(x)}(2\mu+\lambda)u^1)_{hw} + (u^0, D^{(x)}\lambda D^{(y)}v^1)_{hw} \\ &+ (u^0, D^{(y)}\mu D^{(x)}v^1)_{hw} + (u^0, G^{(y)}(\mu)u^1)_{hw}. \end{aligned} \tag{38}$$

The generalization of (6) to two space dimensions with two boundaries gives

$$\begin{aligned} (u^0, G^{(x)}(2\mu+\lambda)u^1)_{hw} &= -(D^{(x)}u^0, (2\mu+\lambda)D^{(x)}u^1)_{hw} - (u^0, P^{(x)}(2\mu+\lambda)u^1)_h \\ &+ \sum_{j=1}^{N_y-1} \left(u^0_{N_x,j}(2\mu+\lambda)_{N_x,j}B^{(x)}u^1_{N_x,j} - u^0_{1,j}(2\mu+\lambda)_{1,j}B^{(x)}u^1_{1,j}\right). \end{aligned} \tag{39}$$

In the y-direction, the same identity holds, but without the boundary terms because of the y-periodic boundary conditions, i.e.,

$$(u^0, G^{(y)}(\mu)u^1)_{hw} = -(D^{(y)}u^0, \mu D^{(y)}u^1)_{hw} - (u^0, P^{(y)}(\mu)u^1)_h. \tag{40}$$

The summation-by-parts property for the first differences gives

$$\begin{aligned}(u^0, D^{(x)}\lambda D^{(y)}v^1)_{hw} = &-(D^{(x)}u^0, \lambda D^{(y)}v^1)_{hw} \\ &+ \sum_{j=1}^{N_y-1} \left(u^0_{N_x,j}\lambda_{N_x,j}D^{(y)}v^1_{N_x,j} - u^0_{1,j}\lambda_{1,j}D^{(y)}v^1_{1,j}\right)\end{aligned}$$

and

$$(u^0, D^{(y)}\mu D^{(x)}v^1)_{hw} = -(D^{(y)}u^0, \mu D^{(x)}v^1)_{hw}. \tag{41}$$

It follows by adding (39)–(41) that

$$\begin{aligned}(u^0, L_h^{(u)}(u^1, v^1))_{hw} = &-(D^{(x)}u^0, (2\mu+\lambda)D^{(x)}u^1)_{hw} - (D^{(y)}u^0, \mu D^{(y)}u^1)_{hw} \\ &- (D^{(x)}u^0, \lambda D^{(y)}v^1)_{hw} - (D^{(y)}u^0, \mu D^{(x)}v^1)_{hw} \\ &- (u^0, P^{(x)}(2\mu+\lambda)u^1)_h - (u^0, P^{(y)}(\mu)u^1)_h \\ &+ \sum_{j=1}^{N_y-1} u^0_{N_x,j}\left((2\mu+\lambda)_{N_x,j}B^{(x)}u^1_{N_x,j} + \lambda_{N_x,j}D^{(y)}v^1_{N_x,j}\right) \\ &- \sum_{j=1}^{N_y-1} u^0_{1,j}\left((2\mu+\lambda)_{1,j}B^{(x)}u^1_{1,j} + \lambda_{1,j}D^{(y)}v^1_{1,j}\right).\end{aligned} \tag{42}$$

Similarly, the second term in (37) becomes

$$\begin{aligned}(v^0, L_h^{(v)}(u^1, v^1))_{hw} = &-(D^{(y)}v^0, (2\mu+\lambda)D^{(y)}v^1)_{hw} - (D^{(x)}v^0, \mu D^{(x)}v^1)_{hw} \\ &- (D^{(y)}v^0, \lambda D^{(x)}u^1)_{hw} - (D^{(x)}v^0, \mu D^{(y)}u^1)_{hw} \\ &- (v^0, P^{(y)}(2\mu+\lambda)v^1)_h - (v^0, P^{(x)}(\mu)v^1)_h \\ &+ \sum_{j=1}^{N_y-1} v^0_{N_x,j}\left(\mu_{N_x,j}B^{(x)}v^1_{N_x,j} + \mu_{N_x,j}D^{(y)}u^1_{N_x,j}\right) \\ &- \sum_{j=1}^{N_y-1} v^0_{1,j}\left(\mu_{1,j}B^{(x)}v^1_{1,j} + \mu_{1,j}D^{(y)}u^1_{1,j}\right).\end{aligned} \tag{43}$$

It is now straightforward to see that the boundary terms in (42) and (43) together form $T_h(\mathbf{u}^0, \mathbf{u}^1)$. Adding together the remaining terms verifies that they equal S_h. The boundary conditions (31), (32), and (33) make $T_h = 0$ when the boundary forcing functions $\tau^{(xx)}$ and $\tau^{(xy)}$ are zero. □

4.1 Time discretization

We discretize time on a uniform grid $t_n = n\Delta_t$, $n = 0, 1, 2, \ldots$, with constant step size $\Delta_t > 0$ and use the notation $\mathbf{u}^n$ for the approximation of $\mathbf{u}(t_n)$. Our time stepping is based on a modified equation approach. Assuming that $\mathbf{u}^n$ and $\mathbf{u}^{n-1}$ satisfy boundary conditions (29)-(33), the following steps are performed to calculate $\mathbf{u}^{n+1}$:

Predictor-corrector time-stepping algorithm:

1. Apply the second order predictor step

$$\rho \frac{\mathbf{u}^* - 2\mathbf{u}^n + \mathbf{u}^{n-1}}{\Delta_t^2} = \mathbf{L}_h(\mathbf{u}^n) + \mathbf{F}(t_n), \tag{44}$$

   to calculate $\mathbf{u}^*$ at all interior points.

2. Impose boundary conditions (29)-(33) on $\mathbf{u}^*$ to define its ghost point values.

3. Apply the corrector step

$$\mathbf{u}^{n+1} = \mathbf{u}^* + \frac{\Delta_t^4}{12}\frac{1}{\rho}\big(\mathbf{L}_h(\mathbf{v}) + \mathbf{F}_{tt}(t_n)\big), \quad \mathbf{v} = \frac{\mathbf{u}^* - 2\mathbf{u}^n + \mathbf{u}^{n-1}}{\Delta_t^2}, \tag{45}$$

   to define $\mathbf{u}^{n+1}$ at all interior points.

4. Impose boundary conditions (29)-(33) on $\mathbf{u}^{n+1}$ to define its ghost point values.

Our analysis of the stability of the predictor-corrector scheme is based on identity (34) and the fact that the bilinear form $S_h(\mathbf{u}, \mathbf{v})$ does not depend on the ghost point values of $\mathbf{u}$ or $\mathbf{v}$. We denote by $\bar{\mathbf{u}}$ a grid function without ghost points that satisfies

$$\bar{\mathbf{u}}_{j,k} = \mathbf{u}_{j,k}, \quad 1 \le j \le N_x, \quad 1 \le k \le N_y - 1.$$

We define a square matrix K such that

$$S_h(\mathbf{u}, \mathbf{v}) = \big(\bar{\mathbf{u}}, \rho K \bar{\mathbf{v}}\big)_{hw}.$$

Because S_h is symmetric, positive semi-definite, and $\rho > 0$, we have

$$\big(\bar{\mathbf{u}}, \rho K \bar{\mathbf{v}}\big)_{hw} = \big(\bar{\mathbf{v}}, \rho K \bar{\mathbf{u}}\big)_{hw}, \quad \big(\bar{\mathbf{u}}, \rho K \bar{\mathbf{u}}\big)_{hw} \ge 0, \quad \text{for all } \bar{\mathbf{u}} \text{ and } \bar{\mathbf{v}}. \tag{46}$$

For all grid functions $\mathbf{u}$ and $\mathbf{v}$ that satisfy boundary conditions (29)-(33) with zero forcing, we have

$$\big(\mathbf{u}, \mathbf{L}_h(\mathbf{v})\big)_{hw} = -S_h(\mathbf{u}, \mathbf{v}) = -\big(\bar{\mathbf{u}}, \rho K \bar{\mathbf{v}}\big)_{hw}.$$

By taking $\mathbf{u} = 0$, except at one interior grid point where $\mathbf{u}_{j,k} = 1$, we can show the point-wise identity

$$\mathbf{L}_h(\mathbf{v}) = -\rho K \bar{\mathbf{v}}, \tag{47}$$

for all $\mathbf{v}$ that satisfy boundary conditions (29)-(33).

Lemma 1. *Let $\mathbf{F}(t) = \mathbf{0}$, $\tau^{(xx)}(t) = 0$, and $\tau^{(xy)}(t) = 0$, for $t \geq 0$. Then the above predictor-corrector scheme is equivalent to*

$$\frac{\bar{\mathbf{w}}^{n+1} - 2\bar{\mathbf{w}}^n + \bar{\mathbf{w}}^{n-1}}{\Delta_t^2} = -\widetilde{K}\bar{\mathbf{w}}^n + \frac{\Delta_t^2}{12}\widetilde{K}^2\bar{\mathbf{w}}^n, \quad \widetilde{K} = \widetilde{K}^T \geq 0, \tag{48}$$

where $\widetilde{K} = Q^{1/2} K Q^{-1/2}$ and $\bar{\mathbf{w}} = Q^{1/2}\bar{\mathbf{u}}$. The diagonal matrix $Q = \rho\Omega > 0$ is defined by the weights in the scalar product

$$\left(\bar{\mathbf{u}}, \bar{\mathbf{v}}\right)_{hw} = \left(\bar{\mathbf{u}}, \Omega\bar{\mathbf{v}}\right)_h. \tag{49}$$

Proof. Since $\mathbf{F}(t_n) = 0$ and $\mathbf{u}^n$ satisfies the boundary conditions with zero forcing, the predictor step is equivalent to

$$\frac{\bar{\mathbf{u}}^* - 2\bar{\mathbf{u}}^n + \bar{\mathbf{u}}^{n-1}}{\Delta_t^2} = -K\bar{\mathbf{u}}^n. \tag{50}$$

Since $\mathbf{u}^*$ and $\mathbf{v}$ satisfy the boundary conditions, the corrector step becomes

$$\bar{\mathbf{u}}^{n+1} = \bar{\mathbf{u}}^* - \frac{\Delta_t^4}{12} K \left(\frac{\bar{\mathbf{u}}^* - 2\bar{\mathbf{u}}^n + \bar{\mathbf{u}}^{n-1}}{\Delta_t^2} \right) = \bar{\mathbf{u}}^* + \frac{\Delta_t^4}{12} K^2 \bar{\mathbf{u}}^n. \tag{51}$$

Eliminating $\bar{\mathbf{u}}^*$ between (50) and (51) gives

$$\frac{\bar{\mathbf{u}}^{n+1} - 2\bar{\mathbf{u}}^n + \bar{\mathbf{u}}^{n-1}}{\Delta_t^2} = -K\bar{\mathbf{u}}^n + \frac{\Delta_t^2}{12} K^2 \bar{\mathbf{u}}^n. \tag{52}$$

Multiplying (52) by $Q^{1/2}$ from the left and introducing $\bar{\mathbf{w}} = Q^{1/2}\bar{\mathbf{u}}$ leads to (48). It remains to show that $\widetilde{K} = \widetilde{K}^T \geq 0$. From the definition of Q, $\widetilde{K}$, and (49), we have

$$\begin{aligned}
\left(\bar{\mathbf{u}}, \rho K \bar{\mathbf{v}}\right)_{hw} &= \left(\bar{\mathbf{u}}, \rho\Omega K \bar{\mathbf{v}}\right)_h = \left(\bar{\mathbf{u}}, QK\bar{\mathbf{v}}\right)_h = \left(Q^{1/2}\bar{\mathbf{u}}, \widetilde{K} Q^{1/2}\bar{\mathbf{v}}\right)_h, \\
\left(\bar{\mathbf{v}}, \rho K \bar{\mathbf{u}}\right)_{hw} &= \left(\bar{\mathbf{v}}, \rho\Omega K \bar{\mathbf{u}}\right)_h = \left(\bar{\mathbf{v}}, QK\bar{\mathbf{u}}\right)_h = \left(Q^{1/2}\bar{\mathbf{v}}, \widetilde{K} Q^{1/2}\bar{\mathbf{u}}\right)_h.
\end{aligned}$$

The first relation in (46) shows that $\widetilde{K} = \widetilde{K}^T$. The second shows that $\widetilde{K}$ is positive semi-definite. □

Since $\widetilde{K}$ is a symmetric positive semi-definite matrix, it has a complete set of eigenvectors corresponding to real eigenvalues $\kappa_j \geq 0$. We can therefore make an eigenvector decomposition of the solution. The stability properties of (48) can therefore be studied by analyzing the scalar second order difference equation

$$\frac{u^{n+1} - 2u^n + u^{n-1}}{\Delta_t^2} = -\kappa u^n + \frac{\Delta_t^2}{12}\kappa^2 u^n, \quad \kappa \geq 0. \tag{53}$$

We make the ansatz

$$u^n = u_0 \xi^n, \quad \xi \in \mathbb{C},$$

leading to the characteristic equation

$$\xi^2 + \xi\big(\kappa\Delta_t^2 - \frac{\kappa^2\Delta_t^4}{12} - 2\big) + 1 = 0. \tag{54}$$

Let $a = \kappa\Delta_t^2 - \kappa^2\Delta_t^4/12 \geq 0$. The roots of (54) are

$$\xi_\pm = 1 - \frac{a}{2} \pm \frac{1}{2}\sqrt{a^2 - 4a}.$$

We have two cases:

1. $a^2 - 4a = a(a-4) > 0$. Then $a > 4$ and

$$\xi_- = 1 - \frac{a}{2} - \frac{\sqrt{a}}{2}\sqrt{a-4} < -1.$$

   Thus, the scheme is unstable.

2. $0 \leq a \leq 4$. Now $a^2 - 4a \leq 0$ and we get complex conjugated roots,

$$\xi_\pm = 1 - \frac{a}{2} \pm \frac{i}{2}\sqrt{4a - a^2}, \quad |\xi_\pm| = 1.$$

We conclude that the scheme (53) is stable for

$$0 \leq \kappa\Delta_t^2 - \kappa^2\Delta_t^4/12 \leq 4. \tag{55}$$

The double inequality leads us to study the zeros of the polynomials

$$P_1(\eta) = \eta - \frac{\eta^2}{12} - 4, \quad P_2(\eta) = \eta - \frac{\eta^2}{12}, \quad \eta = \kappa\Delta_t^2 \geq 0.$$

We have $P_1(0) = -4$ and $P_1'(\eta) = 1 - \eta/6$. Hence, $P_1'(0) = 1$ and

$$P_1'(\eta_*) = 0, \quad \eta_* = 6, \quad P(\eta_*) = -1.$$

Since $P_1''(\eta_*) = -1/6$ this is a global maximum, and we have $P_1(\eta) \leq -1$ for all $\eta \geq 0$.

We have $P_2(\eta) = 0$ for $\eta = 0$ and $\eta = 12$. Since $P_2'(0) = 1$ and $P_2'(12) = -1$ we have

$$P_2(\eta) \geq 0, \quad 0 \leq \eta \leq 12,$$

We conclude that the double inequality (55) is satisfied for

$$0 \leq \kappa \Delta_t^2 \leq 12, \quad 0 \leq \Delta_t \leq \sqrt{3} \frac{2}{\sqrt{\kappa}}.$$

Hence, the scheme (48) is stable under the time step restriction

$$\Delta_t \leq \frac{2\sqrt{3}}{\max_j \sqrt{\kappa_j}} \tag{56}$$

where κ_j are the eigenvalues of $\widetilde{K}$. Note that this time step restriction is $\sqrt{3}$ larger than for the corresponding second order time-stepping method. However, the spatial operator needs to be evaluated twice per time step, so the predictor-corrector method is nevertheless slightly more expensive than the second order method.

Similar to the second order method, the predictor-corrector method is energy conserving. The following theorem summarizes the properties of the scheme.

Theorem 4. *Let the discrete energy be defined by*

$$e_{n+1/2} = \frac{1}{\Delta_t^2} \left\| \bar{\mathbf{w}}^{n+1} - \bar{\mathbf{w}}^n \right\|_h^2 + \left(\bar{\mathbf{w}}^{n+1}, \widetilde{K} \bar{\mathbf{w}}^n \right)_h - \frac{\Delta_t^2}{12} \left(\bar{\mathbf{w}}^{n+1}, \widetilde{K}^2 \bar{\mathbf{w}}^n \right)_h, \tag{57}$$

The predictor-corrector scheme (44)-(45), subject to boundary conditions (29)-(33) with zero forcing terms, conserves the discrete energy in time

$$e^{n+1/2} = e^{n-1/2}.$$

Furthermore, the energy is positive under the time step restriction (56).

Proof. The energy conserving property can be seen by forming the scalar product between $\bar{\mathbf{w}}^{n+1} - \bar{\mathbf{w}}^{n-1}$ and (48),

$$\left(\bar{\mathbf{w}}^{n+1} - \bar{\mathbf{w}}^{n-1}, \bar{\mathbf{w}}^{n+1} - 2\bar{\mathbf{w}}^n + \bar{\mathbf{w}}^{n-1} \right)_h = \left\| \bar{\mathbf{w}}^{n+1} - \bar{\mathbf{w}}^n \right\|_h^2 - \left\| \bar{\mathbf{w}}^n - \bar{\mathbf{w}}^{n-1} \right\|_h^2.$$

Since $\widetilde{K}$ is symmetric,

$$\begin{aligned}
\left(\bar{\mathbf{w}}^{n+1} - \bar{\mathbf{w}}^{n-1}, \widetilde{K} \bar{\mathbf{w}}^n \right)_h &= \left(\bar{\mathbf{w}}^{n+1}, \widetilde{K} \bar{\mathbf{w}}^n \right)_h - \left(\bar{\mathbf{w}}^n, \widetilde{K} \bar{\mathbf{w}}^{n-1} \right)_h, \\
\left(\bar{\mathbf{w}}^{n+1} - \bar{\mathbf{w}}^{n-1}, \widetilde{K}^2 \bar{\mathbf{w}}^n \right)_h &= \left(\bar{\mathbf{w}}^{n+1}, \widetilde{K}^2 \bar{\mathbf{w}}^n \right)_h - \left(\bar{\mathbf{w}}^n, \widetilde{K}^2 \bar{\mathbf{w}}^{n-1} \right)_h.
\end{aligned}$$

By the definition (57) of the discrete energy we get

$$e_{n+1/2} = e_{n-1/2}.$$

We can re-write the discrete energy (57) by using the identity

$$\begin{aligned}\big(\bar{\mathbf{w}}^{n+1} \pm \bar{\mathbf{w}}^{n}, \widetilde{K}(\bar{\mathbf{w}}^{n+1} \pm \bar{\mathbf{w}}^{n})\big)_h \\ = \big(\bar{\mathbf{w}}^{n+1}, \widetilde{K}\bar{\mathbf{w}}^{n+1}\big)_h \pm 2\big(\bar{\mathbf{w}}^{n+1}, \widetilde{K}\bar{\mathbf{w}}^{n}\big)_h + \big(\bar{\mathbf{w}}^{n}, \widetilde{K}\bar{\mathbf{w}}^{n}\big)_h.\end{aligned}$$

that is,

$$\begin{aligned}4\big(\bar{\mathbf{w}}^{n+1}, \widetilde{K}\bar{\mathbf{w}}^{n}\big)_h \\ = \big(\bar{\mathbf{w}}^{n+1} + \bar{\mathbf{w}}^{n}, \widetilde{K}(\bar{\mathbf{w}}^{n+1} + \bar{\mathbf{w}}^{n})\big)_h - \big(\bar{\mathbf{w}}^{n+1} - \bar{\mathbf{w}}^{n}, \widetilde{K}(\bar{\mathbf{w}}^{n+1} - \bar{\mathbf{w}}^{n})\big)_h.\end{aligned}$$

Hence, (57) can be written

$$\begin{aligned}e_{n+1/2} = \big(\bar{\mathbf{w}}^{n+1} - \bar{\mathbf{w}}^{n}, \left(\frac{1}{\Delta_t^2} - \frac{1}{4}\widetilde{K} + \frac{\Delta_t^2}{48}\widetilde{K}^2\right)\big(\bar{\mathbf{w}}^{n+1} - \bar{\mathbf{w}}^{n}\big)\big)_h \\ + \big(\bar{\mathbf{w}}^{n+1} + \bar{\mathbf{w}}^{n}, \left(\frac{1}{4}\widetilde{K} - \frac{\Delta_t^2}{48}\widetilde{K}^2\right)\big(\bar{\mathbf{w}}^{n+1} + \bar{\mathbf{w}}^{n}\big)\big)_h.\end{aligned}$$

We have $e_{n+1/2} \geq 0$ if

$$\frac{1}{\Delta_t^2} - \frac{1}{4}\widetilde{K} + \frac{\Delta_t^2}{48}\widetilde{K}^2 = -\frac{1}{4\Delta_t^2}P_1(\Delta_t^2\widetilde{K}) \geq 0,$$

and

$$\frac{1}{4}\widetilde{K} - \frac{\Delta_t^2}{48}\widetilde{K}^2 = \frac{1}{4\Delta_t^2}P_2(\Delta_t^2\widetilde{K}) \geq 0.$$

Since the eigenvalues of a matrix polynomial equals the polynomial of the eigenvalues of the matrix, we conclude that the discrete energy (57) is positive semi-definite under the same time step conditions as the scalar difference equation (53), i.e.,

$$0 \leq \Delta_t \leq \sqrt{3}\frac{2}{\max_j \sqrt{\kappa_j}}, \quad \widetilde{K}\mathbf{e}_j = \kappa_j \mathbf{e}_j.$$

□

In general, we do not have a closed form expression for the spectral radius of $\tilde{K}$, $\max_j \kappa_j$. In numerical computations, we instead determine the time step based on Fourier analysis of the problem with homogeneous material and periodic boundary conditions. When this formula is applied locally, it leads to the time step estimate

$$\Delta_t = \frac{c_f h}{\max_{i,j} \sqrt{(3\mu_{i,j} + \lambda_{i,j})/\rho_{i,j}}},$$

where c_f is the CFL number. The corresponding second order discretization is stable for $c_f \leq 1$. The fourth order spatial discretization has a somewhat larger spectral radius, numerically found to be 1.41 times the spectral radius of the second order spatial discretization. For our fourth order discretization, the stability limit would therefore be $c_f \leq \sqrt{3/1.41} \approx 1.46$. For the second order scheme, the time step must be taken about 10 percent smaller when a free surface boundary condition is imposed compared to the spatially periodic case [16]. Accounting for this effect in the fourth order discretization, we obtain the CFL limit $0.9 \times 1.46 \approx 1.31$, which agrees well with the observed stable time step in the numerical experiments in the next section.

5 Numerical examples

We here solve the elastic wave equation (20), (21) with the new energy conserving fourth order accurate scheme described in the previous section.

5.1 Method of manufactured solutions

We start by evaluating the error in the numerical solution, when both the material properties and the solution are smooth. The computational domain is $0 \leq x \leq 2\pi$, $0 \leq y \leq 2\pi$, with a free surface boundary conditions on the $x = 0$ boundary, a Dirichlet condition on $x = 2\pi$, and periodic boundary conditions in the y-direction. The material properties are

$$\begin{aligned} \rho(x,y) &= 2 + \sin(x+\phi)\sin(y-\theta), \\ \mu(x,y) &= 3 + \sin(3x+\phi_m)\sin(y) \\ \lambda(x,y) &= 21 + \cos(x+\phi_m)\sin^2(3y), \end{aligned}$$

where $\phi = 0.3$, $\theta = 0.2$, and $\phi_m = 0.1$. The internal forcing, boundary forcing and initial conditions are chosen such that the exact (manufactured) solution becomes

$$\begin{aligned} u_e(x,y,t) &= \cos(x+\phi)\sin(y+\theta)\cos(t^2), \\ v_e(x,y,t) &= \sin(x+\theta)\cos(y+\theta)\sin(t). \end{aligned} \tag{58}$$

Table 1 gives the errors in the numerical solution, evaluated in maximum norm and L^2 norm at different grid resolutions at time $t = 1.0$. The maximum norm is computed over all grid points in the domain and over the two components of the solution. Similarly, the discrete L^2-norm is computed both over the domain and over the two solution components. In both norms, the numerical solution convergences towards the exact solution as $\mathcal{O}(h^4)$.

N_x	h	$\|\mathbf{u}(\cdot,t)-\mathbf{u}_e(\cdot,t)\|_\infty$	$\|\mathbf{u}(\cdot,t)-\mathbf{u}_e(\cdot,t)\|_2$	p_∞	p_2
33	$1.96\cdot 10^{-1}$	$2.94\cdot 10^{-3}$	$5.67\cdot 10^{-4}$	–	–
65	$9.82\cdot 10^{-2}$	$1.72\cdot 10^{-4}$	$2.97\cdot 10^{-5}$	4.09	4.25
129	$4.90\cdot 10^{-2}$	$9.50\cdot 10^{-6}$	$1.56\cdot 10^{-6}$	4.18	4.25
257	$2.45\cdot 10^{-2}$	$5.49\cdot 10^{-7}$	$8.87\cdot 10^{-8}$	4.11	4.13

Table 1: Errors in the numerical solution at time $t = 1.0$, on a uniform grid, when the exact solution is (58). Here, p_∞ and p_2 are the convergence exponents in the maximum norm and 2-norm, respectively.

5.2 Mode to mode conversion

Consider a compressional wave of unit amplitude traveling in the negative x-direction in a homogeneous material, with displacement

$$\mathbf{u}^{(in)} = \begin{pmatrix} k \\ \omega \end{pmatrix} e^{i(\xi t + kx + \omega y)}, \quad k = \cos\phi > 0, \quad \omega = \sin\phi, \quad \xi > 0.$$

If this wave encounters a free surface boundary at $x = 0$, it will be reflected and split into two waves that both travel in the positive x-direction,

$$\begin{aligned} \mathbf{u}^{(out)} &= \mathbf{u}^{(P)} + \mathbf{u}^{(S)}, \\ \mathbf{u}^{(P)} &= R_p \begin{pmatrix} -k \\ \omega \end{pmatrix} e^{i(\xi t - kx + \omega y)}, \\ \mathbf{u}^{(S)} &= \frac{R_s}{\sqrt{\alpha^2 k^2 + \omega^2}} \begin{pmatrix} -\omega \\ -\alpha k \end{pmatrix} e^{i(\xi t - \alpha k x + \omega y)}, \quad \alpha > 0. \end{aligned}$$

The reflected waves correspond to a compressional and a shear wave, since the curl of $\mathbf{u}^{(P)}$ and the divergence of $\mathbf{u}^{(S)}$ are zero. For simplicity, we scale time to give unit density, i.e., $\rho = 1$. In order for $\mathbf{u}^{(in)}$ and $\mathbf{u}^{(out)}$ to satisfy the elastic wave equation (20)-(21) with $f^{(x)} = f^{(y)} = 0$, the frequency and wave numbers must satisfy the elementary relations

$$\xi^2 = (\lambda + 2\mu)(k^2 + \omega^2) = \lambda + 2\mu, \quad \xi^2 = \mu(\alpha^2 k^2 + \omega^2). \tag{59}$$

We have selected the signs of ξ and α such that $\mathbf{u}^{(in)}$ and $\mathbf{u}^{(out)}$ travel in the negative and positive x-direction, respectively. The amplitudes of the reflected waves, R_p and R_s, are functions of λ, μ, and the angle of the incident wave, ϕ. The amplitudes R_p

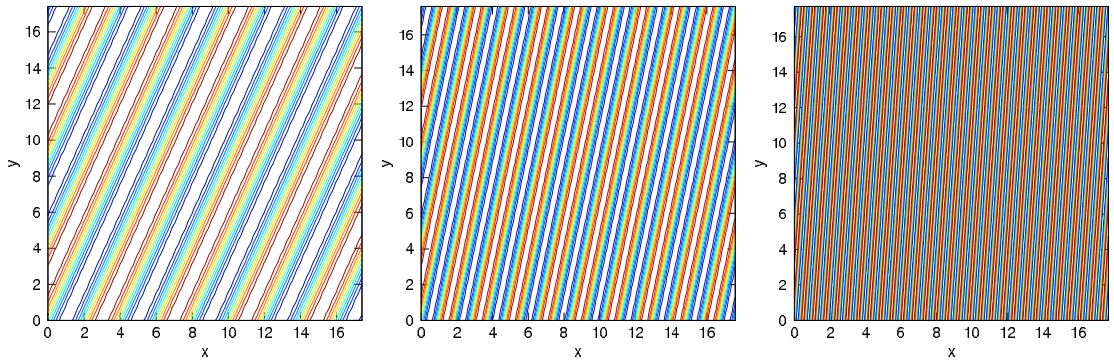

Figure 1: v-component of the outgoing shear wave as function of (x, y) at $t = 0$. The angle of the incoming P-wave is $\phi = \pi/4$. The frames correspond to $\mu = 1.0$ (left), $\mu = 0.1$ (middle), and $\mu = 0.01$ (right).

and R_s are uniquely determined by the free surface boundary conditions (23)-(24) (with $\tau^{(xx)} = \tau^{(xy)} = 0$).

As a consequence of the relation (59),

$$\alpha^2 = 1 + \frac{\lambda + \mu}{\mu \cos^2 \phi}.$$

Hence, when $\mu \ll \lambda$, the reflected S-wave will propagate almost parallel to the x-direction because $\alpha^2 \gg 1$, see Figure 1. The wave lengths of the compressional and shear waves are given by

$$L_p = \frac{2\pi}{\sqrt{k^2 + \omega^2}} = 2\pi, \quad L_s = 2\pi \sqrt{\frac{\mu}{\lambda + 2\mu}}.$$

Note that the wave length of the compressional wave is fixed, while L_s becomes small as $\mu \to 0$.

To include two wave lengths of $\mathbf{u}^{(in)}$ in the computational domain, we take $L_y = 4\pi/\sin\phi$ and $L_x = 4\pi/\cos\phi$. As before, we impose periodic boundary conditions in the y-direction, a Dirichlet boundary condition at $x = L_x$ and a free surface condition at $x = 0$. By construction, the function $\mathbf{u}^{(in)} + \mathbf{u}^{(out)}$ is L_y-periodic in the y-direction, satisfies the elastic wave equation in the interior, and the free surface condition at $x = 0$. In principle, we could compute a numerical approximation of $\mathbf{u}^{(in)} + \mathbf{u}^{(out)}$ by adding a suitable forcing function to the Dirichlet boundary condition at $x = L_x$. However, we instead choose to only compute the outgoing S-wave, $\mathbf{u}^{(S)}$. For this reason, we impose the inhomogeneous Dirichlet boundary condition

$$\mathbf{u}(L_x, y, t) = \mathbf{u}^{(S)}(L_x, y, t),$$

and take the forcing functions in the normal stress boundary conditions (23)-(24) to be

$$\tau^{(xx)} = -(2\mu+\lambda)\left(u_x^{(in)} + u_x^{(P)}\right) - \lambda\left(v_y^{(in)} + v_y^{(P)}\right),$$
$$\tau^{(xy)} = -\mu\left(u_y^{(in)} + u_y^{(P)} + v_x^{(in)} + v_x^{(P)}\right).$$

We use the exact solution $\mathbf{u}^{(S)}$ as initial conditions for the numerical solution.

To accurately solve this problem numerically, it is necessary to resolve the short shear waves on the computational grid. For this problem, we define the resolution in terms of the number of grid points per shear wave length,

$$P_s = \frac{L_s}{h} = \frac{\sqrt{\mu}}{h}\frac{2\pi}{\sqrt{\lambda+2\mu}}.$$

We evaluate the error in the numerical solution as function of time for two materials. The first material has ($\lambda = 1$, $\mu = 0.1$) and the second has ($\lambda = 1$, $\mu = 0.01$). As a consequence, the period of the wave is slightly different for the two cases

$$T = \frac{2\pi}{\xi} = \frac{2\pi}{\sqrt{\lambda+2\mu}} \approx \begin{cases} 5.74, & \mu = 0.1, \\ 6.22, & \mu = 0.01. \end{cases}$$

In Figure 2 we show the error as function of normalized time, t/T, for the two materials. Note that the error levels are comparable for the same number of grid points per wave length, and converge to zero as $\mathcal{O}(P_s^{-4})$ as the grid is refined. However, to keep the number of grid points per wave length constant for different materials, we have to choose the grid size according to

$$h = \frac{2\pi}{\sqrt{\lambda+2\mu}}\frac{\sqrt{\mu}}{P_s}.$$

Compared to the material with $\mu = 0.1$, the grid size must therefore be taken about a factor of $\sqrt{10}$ smaller for the case $\mu = 0.01$, to obtain the same number of grid points per wave length. Hence, the total number of grid points in a two-dimensional calculation grows as $\mathcal{O}(\mu^{-1})$ as $\mu \to 0$, while the number of time steps per period grows as $\mathcal{O}(\mu^{-1/2})$. Note that this asymptotic scaling is valid for any numerical method that requires a fixed number of grid points per wave length. In particular, the exponents are independent of the order of accuracy.

5.3 Surface waves

A Rayleigh surface wave satisfies the elastic wave equation in a homogeneous half-space subject to a free surface condition on the boundary. For simplicity we scale

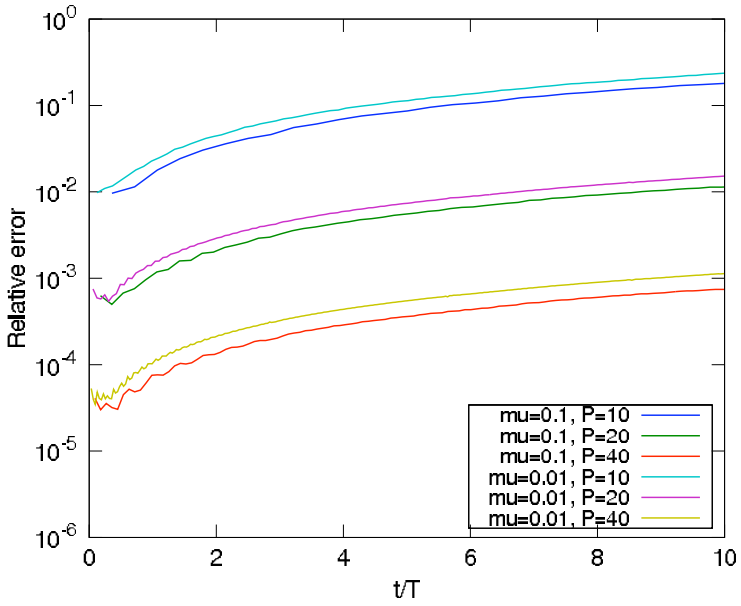

Figure 2: Results for computing the outgoing shear wave with different resolution, characterized by the number of grid points per wave length, P_s. The relative error in max norm is shown as function of time scaled by the period of the wave. Two cases are shown, ($\lambda = 1$, $\mu = 0.1$) and ($\lambda = 1$, $\mu = 0.01$).

time to give unit density, $\rho = 1$. For the y-periodic half-space $x \geq 0$, the surface wave can be written

$$\mathbf{u}_s(x,y,t) = e^{-\omega x\sqrt{1-\tilde{\xi}^2}} \begin{pmatrix} \cos\big(\omega(y+c_r t)\big) \\ \sqrt{1-\tilde{\xi}^2}\sin\big(\omega(y+c_r t)\big) \end{pmatrix} + \left(\frac{\tilde{\xi}^2}{2}-1\right) e^{-\omega x\sqrt{1-\tilde{\xi}^2\mu/(2\mu+\lambda)}} \begin{pmatrix} \cos\big(\omega(y+c_r t)\big) \\ \sin\big(\omega(y+c_r t)\big)/\sqrt{1-\tilde{\xi}^2\mu/(2\mu+\lambda)} \end{pmatrix}, \quad (60)$$

where $\omega > 0$. We define the Rayleigh phase velocity by

$$c_r = \tilde{\xi}\sqrt{\mu},$$

where $\tilde{\xi}$ satisfies the dispersion relation

$$\sqrt{1-\tilde{\xi}^2}\sqrt{1-\frac{\mu\tilde{\xi}^2}{\lambda+2\mu}} - \left(1-\frac{\tilde{\xi}^2}{2}\right)^2 = 0.$$

It is straight forward to verify that $0.763 < \tilde{\xi}^2 < 0.913$ for all materials with $\mu > 0$ and $\lambda \geq 0$. Hence, the surface wave propagates in the y-direction and decays

exponentially in x. Its phase velocity is always slower than that of a shear wave, $c_s = \sqrt{\mu}$.

The wave length of the surface wave is $L_r = 2\pi/|\omega|$, and we define the number of grid points per wave length by

$$P_r = \frac{L_r}{h}.$$

In this investigation we shall keep the wave length fixed at $L_r = 1$, which gives the spatial frequency $\omega = 2\pi$. We let the computational domain contain exactly one wave length of the solution by taking $L_y = L_r = 1$. A free surface boundary condition is imposed at $x = 0$. We truncate the computational domain at $x = L_x = 10$ by an inhomogeneous Dirichlet condition where the exact solution is prescribed as forcing.

In our first experiment, we take $\mu = 0.01$. The numerical solution is evolved from initial data given by (60) at time $t = 0$ and $t = -\Delta_t$, where the time step satisfies the Courant condition (recall that we have scaled time to give unit density)

$$\Delta_t = \frac{1.3\, h}{\sqrt{\lambda + 3\mu}}.$$

In Figure 3 we show the max norm of the error in the numerical solution as function of time for $t \leq 20$. Since the wave length in the y-direction is one, the number of grid points per wave length satisfies $P = N_y - 1$. The error measured in max norm decreases by a factor of 16 when the number of grid points is doubled. Note that about 20 grid points per wave length are needed to make the error less than about 5% of the exact solution.

In our next experiment, we study the accuracy of the Rayleigh wave (60) for different values of μ. The period of the wave is

$$T = \frac{2\pi}{\omega c_r} = \frac{1}{c_r} = \frac{1}{\tilde{\xi}\sqrt{\mu}}. \tag{61}$$

In the following table we list the period for some values of μ.

μ	1	0.1	0.01	0.001
T	1.087	3.330	10.474	33.104

Note that the period gets longer, i.e., the surface wave propagates slower as $\mu \to 0$.

In Figure 4 we show the max error in the numerical solution after one period, i.e., at time $t = T$, for $\lambda = 1$ and different values of μ. As the grid is refined, the error decays as $\mathcal{O}(P_r^{-4})$ for all values of μ. However, for a fixed number of grid points per wave length, the error becomes larger as $\mu \to 0$.

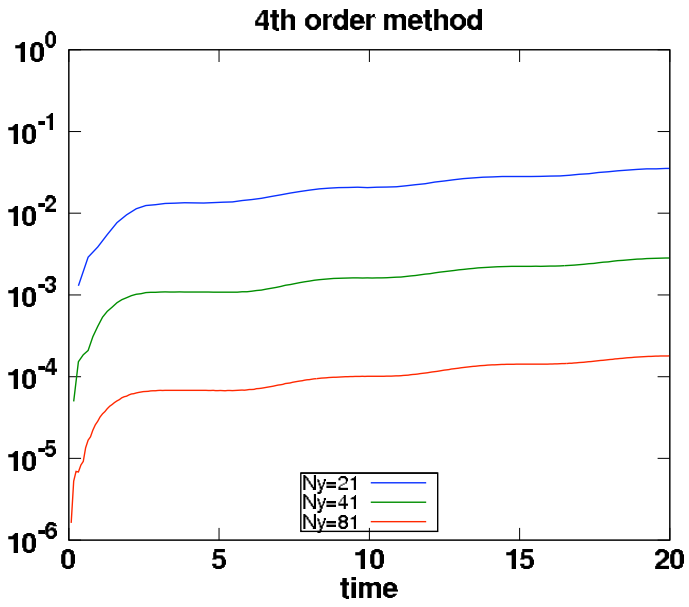

Figure 3: Max error as function of time for a Rayleigh surface wave with $\lambda = 1$ and $\mu = 0.01$. The different lines correspond to different number of grid points per wave length; $P_r = 20$ (blue), $P_r = 40$ (green), and $P_r = 80$ (red).

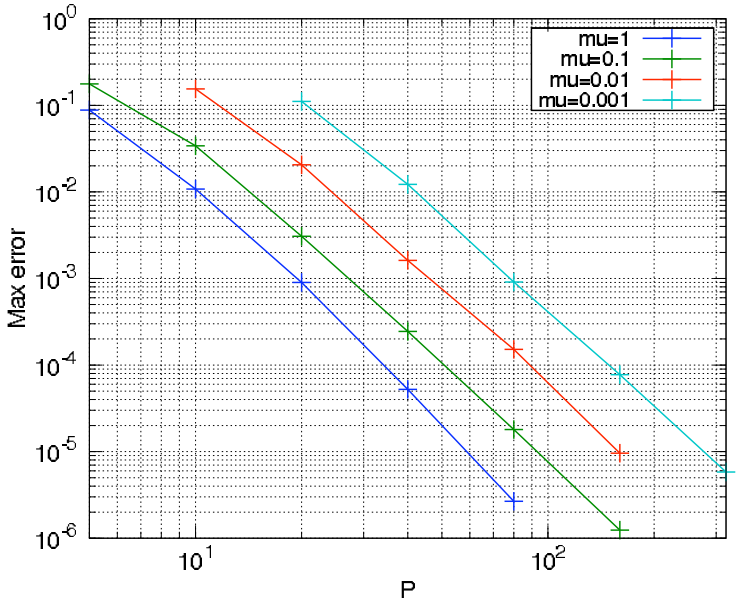

Figure 4: Error in maximum norm in the numerical evolution of the Rayleigh surface wave after one period, as function of the number of grid points per wave length, P_r. The different curves correspond to $\mu = 1$ (blue), $\mu = 0.1$ (green), $\mu = 0.01$ (red), and $\mu = 0.001$ (cyan).

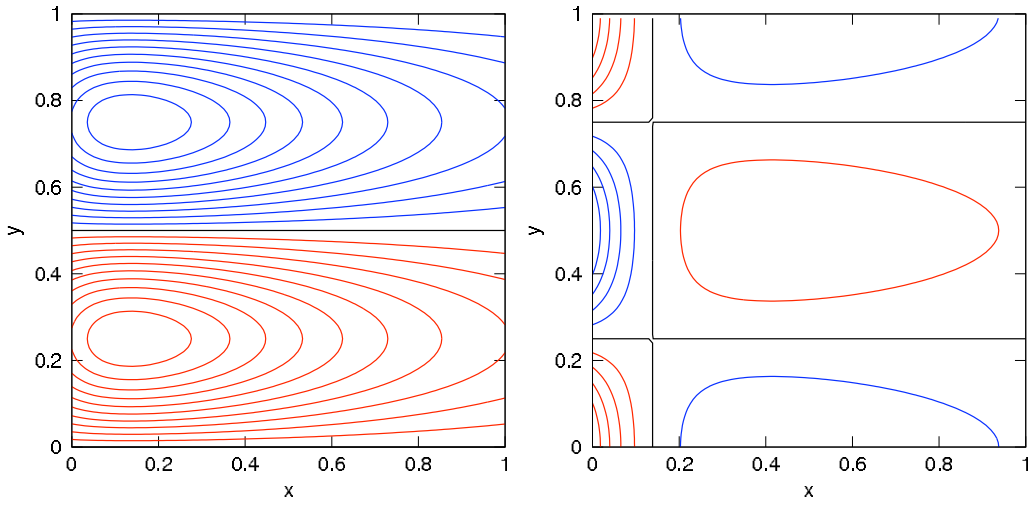

Figure 5: The Rayleigh surface wave as function of (x, y) at $t = 0$ for $\mu = 0.01$. The u-component is shown to the left and the v-component to the right. The contour lines are plotted at levels between -0.5 and 0.5, with spacing 0.05. Red and blue lines correspond to negative and positive values, respectively. The zero level is plotted in black.

We remark that the loss of accuracy as $\mu \to 0$ is not due to poor spatial resolution. In the x-direction, the gradient of the exact solution is the largest along the $x = 0$ boundary, with P_r grid points per wave length. The gradient in the y-direction is also the largest along the boundary and is of the same order as the x-gradient of the solution, see Figure 5. Furthermore, the phase velocity of the surface wave becomes slower and slower as $\mu \to 0$, while the time step is governed by $\sqrt{\lambda + 3\mu}$, which tends to $\sqrt{\lambda} = 1$. Hence, the temporal resolution of the surface wave only improves as $\mu \to 0$.

The poor accuracy for small μ can be explained by a normal mode analysis, see Kreiss and Petersson [11]. Truncation errors lead to a perturbed phase velocity of the surface wave, which can be modeled by a modified equation technique. According to this theory, for small μ, the error in the numerical solution after one period satisfies

$$\varepsilon = \frac{C}{P_r^4 \mu}, \quad C = \text{const.}, \quad \mu \to 0. \tag{62}$$

We test this theory by plotting the max error after one period as function of $P_r \mu^{1/4}$, see Figure 6. We conclude that the errors follow (62) remarkably well, especially for the three smaller values of μ. The case $\mu = 1$ appears to be too large for (62) to apply.

Figure 7 demonstrates the superior efficiency of higher order methods over lower order methods. Figure 7 was obtained by solving the elastic wave equation to a fixed

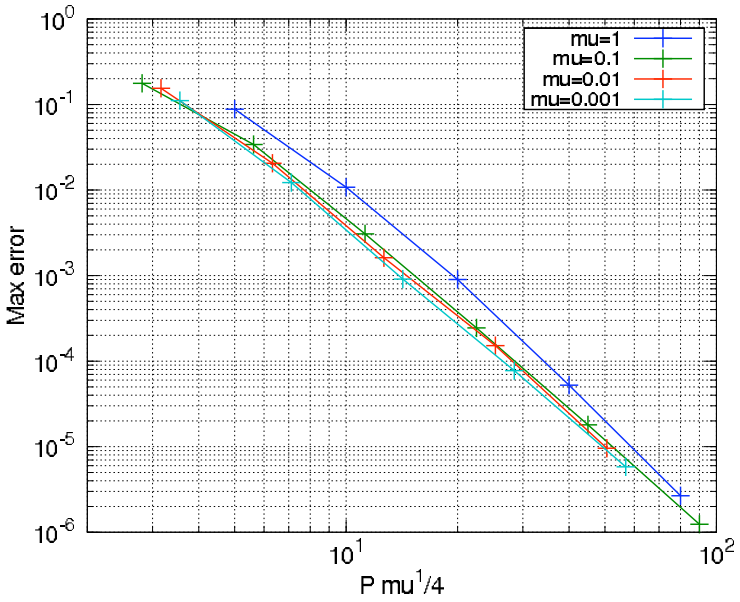

Figure 6: Max error in the numerical evolution of the Rayleigh surface wave after one period, as function of $P_r\mu^{1/4}$. The different curves correspond to $\mu = 1$ (blue), $\mu = 0.1$ (green), $\mu = 0.01$ (red), and $\mu = 0.001$ (cyan).

time on a set of grids with different number of grid points. For each computation, the CPU time used and the maximum norm of the relative error of the solution at the final time was recorded. The computations were made with both the new fourth order method and with our previously developed second order method. Figure 7 shows the solution error vs. CPU time, in logarithmic scale, for the two methods and the two cases $\mu = 1$ and $\mu = 0.001$. The figure shows that the fourth order method is more efficient than the second order method over the entire range of problem sizes, and that the advantage for the high order method increases as the required error tolerance is made smaller.

For example, in the case $\mu = 0.001$, a solution error of size 10^{-4} can be obtained in 34 seconds of CPU time with the fourth order method. By extrapolating the data for the second order method, we estimate that a solution with the same error would require 1.92×10^5 CPU seconds, i.e., more than 54 hours of computing. The gain in efficiency depends on the exact details of the implementation, the compiler and compiler settings, and the hardware used. However, based on our experience, the performance shown in Figure 7 is generally valid in a qualitative sense.

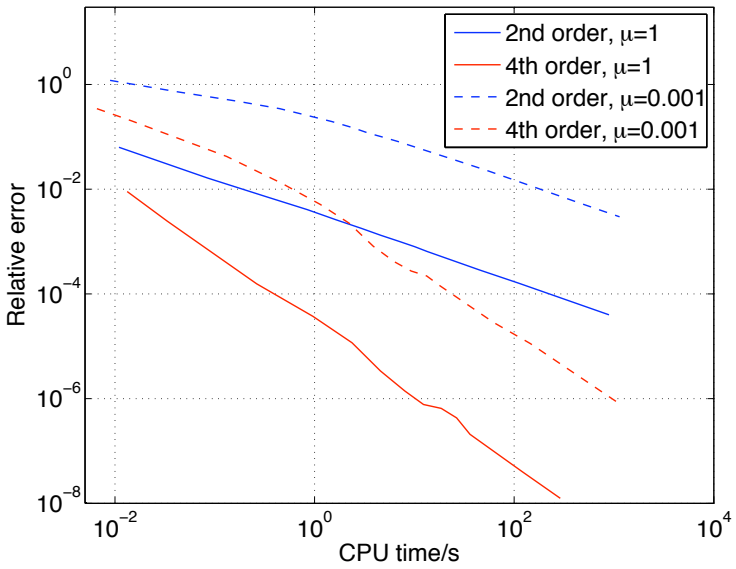

Figure 7: Maximum norm relative errors at time 1.088 in the numerical evolution of the Rayleigh surface wave vs. CPU time for second order (blue) and fourth order accurate (red) finite difference schemes. The different curves correspond to $\mu = 1$ (solid) and $\mu = 0.001$ (dashes). Here $\rho = 1$ and $\lambda = 1$.

6 Conclusions

We have presented a fourth order accurate finite difference method for the two-dimensional elastic wave equation in second order formulation, where the fourth order accuracy holds in both space and time. The spatial discretization satisfies the summation by parts principle and allows for heterogeneous materials and free surface boundary conditions. The key ingredient of the method is a boundary modified fourth order accurate discretization of the second derivative with variable coefficient, $(\mu(x)u_x)_x$, which is consistent with the discretization of cross-terms such that an energy estimate can be obtained. In contrast to previous summation by parts operators, we design the discretization to use one ghost point outside the physical boundary. This allows boundary conditions to be enforced in a point wise manner, and avoids the use of projections or penalty terms. The explicit temporal discretization is fourth order accurate and energy conserving. Numerical examples with free surface boundary conditions show that the scheme is stable for CFL-numbers up to 1.3.

Preliminary analysis indicates that sixth and eighth order accurate discretizations of $(\mu(x)u_x)_x$ can be derived using a similar approach. These stencils include "free" parameters that must be determined to avoid time-stepping stiffnesses and guarantee stability of the overall discretization. More work is needed to evaluate if

these very high order methods are more efficient than the fourth order method.

A number of generalizations are needed to make the proposed method useful in practical applications. To get capabilities for simulating seismic waves, similar to the second order accurate finite difference method implemented in WPP [18], the proposed method would need a number of enhancements. The method would first need to be generalized to three-dimensional domains. A non-planar topography could be handled using the curvilinear mesh technique described in [1]. Singular source terms would need to be discretized to fourth order accuracy, for example by generalizing the technique described in [20]. Energy conserving interface conditions at grid refinement boundaries could in principle be handled in the same way as in [20], but it is not obvious what order of accuracy the solution will get in this case. Visco-elastic material modeling could be generalized to fourth order accuracy using the same technique as in [19], and far field boundary conditions could be handled as described in [17].

The summation by part principle is a generally applicable technique and prescribes a provably stable difference approximation of a partial differential equation that satisfies an energy estimate. Hence, the proposed fourth order discretization of second derivatives could also be used to obtain stable fourth order accurate discretizations of other partial differential equations, besides the elastic wave equation.

A Coefficients

The coefficients of the truncation error of $D(\mu Du)$ in (14) are

$$\begin{aligned} &c_1 = 543301/608923, \quad c_2 = 147/731, \qquad c_3 = -19259/107457, \\ &c_4 = -19/15351, \qquad c_5 = 3539/151704, \quad c_6 = -11/3528. \end{aligned}$$

The coefficients of the truncation error of Du in (15) are

$$d_1 = -43/102, \quad d_2 = 1/6, \quad d_3 = -5/258, \quad d_4 = -11/294.$$

B Derivation of the solution of (16)

Write (16) as

$$M\alpha + \widetilde{\Omega}\mathbf{c} + \mathbf{g} = \mathbf{0}, \tag{63}$$

with

$$M = \begin{pmatrix} 1 & 0 & 0 & 0 \\ -2 & 1 & 0 & 0 \\ 1 & -2 & 1 & 0 \\ 0 & 1 & -2 & 1 \\ 0 & 0 & 1 & -2 \\ 0 & 0 & 0 & 1 \end{pmatrix},$$

and

$$\widetilde{\Omega} = diag(\omega_1\ \omega_2\ \omega_3\ \omega_4\ 1\ 1).$$

Here, α is the column vector formed by the four α_j, $\mathbf{c}$ is the column vector formed by the six c_j, and $\mathbf{g} = (d_1\ 0\ 0\ 0\ 0\ 0)^T$. Partition M, $\widetilde{\Omega}$, and $\mathbf{g}$ into two blocks each,

$$M = \begin{pmatrix} M_1 \\ M_2 \end{pmatrix}, \quad \widetilde{\Omega} = \begin{pmatrix} \widetilde{\Omega_1} \\ \widetilde{\Omega_2} \end{pmatrix}, \quad \mathbf{g} = \begin{pmatrix} \mathbf{g}_1 \\ \mathbf{0} \end{pmatrix},$$

where M_1 consists of the first two rows of M and M_2 is the 4×4 matrix formed by the last four rows of M. Similarly, $\widetilde{\Omega_1}$ has two rows and six columns, $\widetilde{\Omega_2}$ has size 4×6, and $\mathbf{g}_1 = (d_1\ 0)^T$. The solution of the four last equations is

$$\alpha = -M_2^{-1}\widetilde{\Omega}_2\mathbf{c},$$

which uniquely determines α, since M_2 is non-singular. The condition for solvability of (63), obtained by inserting this α into the first two equations, becomes

$$M_1 M_2^{-1}\widetilde{\Omega}_2\mathbf{c} = \widetilde{\Omega}_1\mathbf{c} + \mathbf{g}_1.$$

After explicitly evaluating $M_1 M_2^{-1}$, we can write the above system as

$$\begin{pmatrix} -1 & 0 & 1 & 2 & 3 & 4 \\ 0 & -1 & -2 & -3 & -4 & -5 \end{pmatrix} \widetilde{\Omega}\mathbf{c} = \mathbf{g}_1.$$

We will denote the two rows of the above matrix by $\mathbf{m}_1^T$ and $\mathbf{m}_2^T$. Next, observe that $c = Dd$ where c and d are the grid functions of the leading order truncation error coefficients defined in (14) and (15) respectively. This relation follows from the definition of the c_j as the leading order truncation error coefficients of the second difference operator D^2. We therefore obtain,

$$\begin{pmatrix} \mathbf{m}_1^T \\ \mathbf{m}_2^T \end{pmatrix} \widetilde{\Omega}\widetilde{D}\mathbf{d} = \mathbf{g}_1 \tag{64}$$

where $\mathbf{d}$ consists of $d_1, \ldots, d_8$ and $\widetilde{D}$ is the 6×8 matrix formed by the summation by parts operator at the grid points $j = 1, \ldots, 6$. The summation by parts property (7) gives

$$m_k^T \Omega D d = -d^T \Omega D m_k - d_1 m_{k,1}, \qquad k = 1, 2. \tag{65}$$

where m_k denotes the grid function obtained by extending the vector $\mathbf{m}_k$ to all grid points by padding it with zero elements. Let $m_{k,j}$ denote the jth element of the grid function m_k. Since, $m_{1,1} = -1$ and $m_{2,1} = 0$, (65) is equivalent to (64) if

$$d^T \Omega D m_k = 0, \quad k = 1, 2. \tag{66}$$

Now, for $j = 1, \ldots, 6$, m_k are linear functions of j (and equivalently of x_j) and consequently Dm_k is constant for $j = 1, \ldots, 4$, and when $j \geq 5$, $d_j = 0$. This implies that (66) is equivalent with

$$(e, d)_{hw+} = h \sum_{j=1}^{4} d_j \omega_j = 0, \tag{67}$$

i.e., the truncation error coefficients are orthogonal to the norm weights on the boundary. Here, e denotes the grid function with $e_j = 1$ for all j.

We will next integrate polynomials. Integrals of polynomials over the domain $0 \leq x < \infty$ are not convergent. Therefore, we will here temporarily consider the case of a bounded domain, discretized by x_j, $j = 1, \ldots, N$, with a summation by parts scalar product $(u, v)_{hw}$ and finite difference operator D, that are boundary modified at both boundaries. To prove (67), take $u = x^3/6$ to obtain the exact relation

$$Du_j = x_j^2/2 + h^2 d_j, \quad j = 1, \ldots, N.$$

It follows that

$$(e, Du)_{hw} = (e, x^2/2)_{hw} + h^2 (e, d)_{hw}.$$

The summation by parts property gives

$$(e, Du)_{hw} = -(De, u)_{hw} - u_1 + u_N = -u_1 + u_N$$

and integration by parts show $\int_{x_1}^{x_N} u_x \, dx = (e, u_x) = -u_1 + u_N$ for any smooth function $u(x)$, and $e(x) = 1$ so that

$$(e, x^2/2) = (e, x^2/2)_{hw} + h^2 (e, d)_{hw}.$$

Lemma 2 below proves that the weighted norm, $(e, u)_{hw}$, is a fourth order quadrature formula, i.e., $(e, u)_{hw}$ is an exact formula for the corresponding integral when u is a polynomial of degree ≤ 3. Therefore $(e, x^2/2)_{hw} = (e, x^2/2)$ exactly, which implies that $(e, d)_{hw} = 0$. For the fourth order operator D, we have $d_j = 0$ for $5 \leq j \leq N-4$,

and Taylor expansion shows that $d_{N-j+1} = d_j$ for $j = 1, \ldots, 4$. The weights of the scalar product also satisfy the symmetry $\omega_{N-j+1} = \omega_j$, $j = 1, \ldots, 4$. Hence

$$0 = (e, d)_{hw} = 2h \sum_{j=1}^{4} \omega_j d_j.$$

This proves (67) and hence (66) and (64). Note: for summation by parts operators that are of odd order on the boundary, the truncation error coefficients are anti-symmetric, $d_{N-j+1} = -d_j$, and $(e, d)_{hw} = 0$ does not directly imply the orthogonality (67). However, numerical investigations have shown that the property holds also for odd boundary order greater than one.

Lemma 2. *Let D be a summation by parts difference operator whose lowest order of accuracy is p. Then the corresponding summation by parts scalar product is an exact quadrature formula for polynomials up to order $2p-1$, i.e., $(e, x^k)_{hw} = (e, x^k)$ for $k = 0, \ldots, 2p-1$*

Proof. Consider the operator on a bounded interval $a \leq x \leq b$, discretized by N grid points, i.e., $x_1 = a$ and $x_N = b$. pth order of accuracy means that D is exact for polynomials up to degree p. We have

$$Dx_j^s = px_j^{s-1}, \quad j = 1, \ldots, N, \quad 0 < s \leq p.$$

The property (7) on a bounded interval with $u = v$ gives

$$(u, Du)_{hw} = \frac{1}{2}(u_N^2 - u_1^2).$$

Insert the function $u = x^s$ to obtain

$$(x^s, sx^{s-1})_{hw} = \frac{1}{2}(x_N^{2s} - x_1^{2s}).$$

Dividing by s gives

$$(e, x^{2s-1})_{hw} = (x^s, x^{s-1})_{hw} = \frac{1}{2s}(x_N^{2s} - x_1^{2s}).$$

Hence, $(e, x^{2s-1})_{hw}$ is equal to the exact integral $\int_{x_1}^{x_N} x^{2s-1}\, dx$. This proves the Lemma for odd exponents $\leq 2p-1$. For even exponents, we use the same idea, but apply (7) with $u = x^s$ and $v = x^{s+1}$. □

References

[1] D. Appelö and N. A. Petersson. A stable finite difference method for the elastic wave equation on complex geometries with free surfaces. *Comm. Comput. Phys.*, 5:84–107, 2009.

[2] M. H. Carpenter, D. Gottlieb, and S. Abarbanel. Time-stable boundary conditions for finite-difference schemes solving hyperbolic systems: Methodology and application to high-order compact schemes. *J. Comput. Phys.*, 111:220–236, 1994.

[3] M. H. Carpenter, J. Nordström, and D. Gottlieb. A stable and conservative interface treatment of arbitrary spatial accuracy. *J. Comput. Phys.*, 148:341–365, 1999.

[4] M. Dumbser and M. Käser. An arbitrary high-order discontinuous Galerkin method for elastic waves on unstructured meshes - II. the three-dimensional isotropic case. *Geophys. J. Int.*, 167:319–336, 2006.

[5] K.-A. Feng, C.-H. Teng, and M.-H. Chen. A pseudospectral penalty scheme for 2D isotropic elastic wave computations. *J. Sci. Comput.*, 33:313–348, 2007.

[6] R.W. Graves. Simulating seismic wave propagation in 3D elastic media using staggered-grid finite differences. *Bull. Seism. Soc. Am.*, 86:1091–1106, 1996.

[7] B. Gustafsson. The convergence rate for difference approximations to mixed initial boundary value problems. *Math. Comput.*, 29(130):396–406, 1975.

[8] B. Gustafsson, H.-O. Kreiss, and J. Oliger. *Time dependent problems and difference methods*. Wiley–Interscience, 1995.

[9] K. Komatitsch and J. Tromp. Introduction to the spectral element method for three-dimensional seismic wave propagation. *Geophys. J. Int.*, 139:806–822, 1999.

[10] H.-O. Kreiss and J. Oliger. Comparison of accurate methods for the integration of hyperbolic equations. *Tellus*, 24:199–215, 1972.

[11] H.-O. Kreiss and N.A. Petersson. Boundary estimates for the elastic wave equation in almost incompressible materials. LLNL-JRNL 482152, Lawrence Livermore National Laboratory, 2011. Submitted to SIAM J. Numer. Anal.

[12] H.-O. Kreiss and G. Scherer. Finite element and finite difference methods for hyperbolic partial differential equations. In *Mathematical aspects of Finite Elements in Partial differential equations*. Academic Press, 1974.

[13] A.R. Levander. Fourth-order finite-difference P-SV seismograms. *Geophysics*, 53:1425–1436, 1988.

[14] K. Mattson. *Summation-by-Parts Operators for High Order Finite Difference Methods*. PhD thesis, Uppsala University, Information Technology, Department of Scientific Computing, 2003.

[15] K. Mattsson and J. Norström. Summation by parts operators for finite difference approximations of second derivatives. *J. Comput. Phys.*, 199:503–540, 2004.

[16] S. Nilsson, N. A. Petersson, B. Sjögreen, and H.-O. Kreiss. Stable difference approximations for the elastic wave equation in second order formulation. *SIAM J. Numer. Anal.*, 45:1902–1936, 2007.

[17] N. A. Petersson and B. Sjögreen. An energy absorbing far-field boundary condition for the elastic wave equation. *Commun. Comput. Phys.*, 6:483–508, 2009.

[18] N. A. Petersson and B. Sjögreen. Reference guide to WPP version 2.0. Technical Report LLNL-TR-422928, Lawrence Livermore National Laboratory, 2010. (Source code available from https://computation.llnl.gov/casc/serpentine).

[19] N. A. Petersson and B. Sjögreen. Stable and efficient modeling of anelastic attenuation in seismic wave propagation. Technical Report LLNL-JRNL-460239, Lawrence Livermore National Laboratory, 2010. (Submitted to Comm. Comput. Phys.).

[20] N. A. Petersson and B. Sjögreen. Stable grid refinement and singular source discretization for seismic wave simulations. *Commun. Comput. Phys.*, 8:1074–1110, 2010.

[21] B. Sjögreen. High order centered difference methods for the compressible Navier-Stokes equations. *J. Comput. Phys.*, 117:67–78, 1995.

[22] B. Strand. Summation by parts for finite difference approximations for d/dx. *J. Comput. Phys.*, 110:47–67, 1994.

[23] J. Virieux. P-SV wave propagation in heterogeneous media: Velocity-stress finite-difference method. *Geophysics*, 51:889–901, 1986.

[24] L.C. Wilcox, G. Stadler, C. Burstedde, and O. Ghattas. A high-order discontinuous Galerkin method for wave propagation through coupled elastic-acoustic media. *J. Comput. Phys.*, 229:9373–9396, 2010.